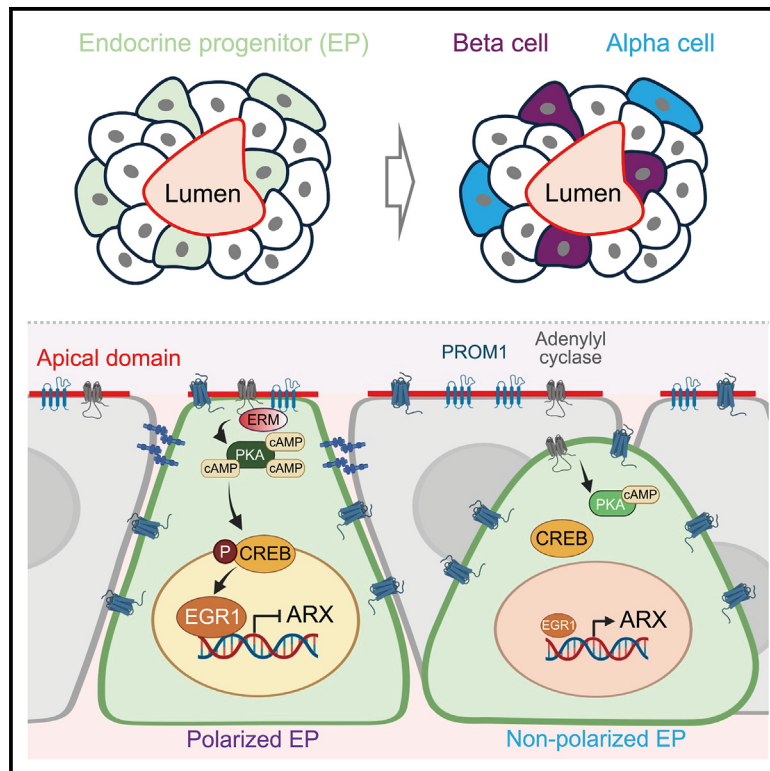


# Developmental Cell

## Pancreatic alpha and beta cell fate choice is directed by apical-basal polarity dynamics

### Graphical abstract



### Authors

Ulf Tiemann, Chenglei Tian (田成磊), Florian Hermann, ..., Yilin Di (狄怡琳), Jakub Sedzinski, Henrik Semb

### Correspondence

henrik.semb@helmholtz-munich.de

### In brief

Tiemann and Tian et al. discover that multipotent pancreatic endocrine progenitors (EPs) differentiation is dictated by apical-basal polarity. In polarized EPs, cAMP increases via the cAMP/PKA-CREB-EGR1 pathway to inhibit ARX and promote beta cell birth, while alpha cells arise from non-polarized EPs, where the absence of cAMP elevation maintains ARX expression.

### Highlights

- Multipotent endocrine progenitors (EPs) dynamically change their polarity status
- Apical-basal polarity of EPs dictates their fate toward alpha and beta cells
- Polarity increases cAMP, leading to beta cell birth via reduced ARX expression
- In non-polarized EPs, ARX expression is maintained, leading to alpha cell birth

Article

# Pancreatic alpha and beta cell fate choice is directed by apical-basal polarity dynamics

Ulf Tiemann,<sup>2,5,6</sup> Chenglei Tian (田成磊),<sup>1,2,5</sup> Florian Hermann,<sup>2</sup> Martin Proks,<sup>3</sup> Emilie Skovgaard,<sup>2</sup> Ivan Kulik,<sup>1,2</sup> Yilin Di (狄怡琳),<sup>1,4</sup> Jakub Sedzinski,<sup>3</sup> and Henrik Semb<sup>1,2,7,\*</sup>

<sup>1</sup>Institute of Translational Stem Cell Research, Helmholtz Diabetes Center, Helmholtz Zentrum Munchen, Munich 85764, Germany

<sup>2</sup>Novo Nordisk Foundation Center for Stem Cell Biology (DanStem), University of Copenhagen, Copenhagen 2200, Denmark

<sup>3</sup>Novo Nordisk Foundation Center for Stem Cell Medicine (reNEW), University of Copenhagen, Copenhagen 2200, Denmark

<sup>4</sup>School of Medicine and Health, Technical University of Munich, Munich 81675, Germany

<sup>5</sup>These authors contributed equally

<sup>6</sup>Present address: Biotech Research and Innovation Centre (BRIC), University of Copenhagen, Copenhagen 2200, Denmark

<sup>7</sup>Lead contact

\*Correspondence: [henrik.semb@helmholtz-munich.de](mailto:henrik.semb@helmholtz-munich.de)

<https://doi.org/10.1016/j.devcel.2025.02.008>

## SUMMARY

A central question in cell and developmental biology is how extracellular cues control the differentiation of multipotent progenitors in a dynamically changing niche. Here, we identify apical-basal polarity as the main regulator of the differentiation of multipotent pancreatic Neurogenin3<sup>+</sup> endocrine progenitors (EPs) into the beta or alpha cell fates. We show that human EPs dynamically change their apical-basal polarity status. Whereas polarized EPs are predisposed to differentiate into beta cells rather than alpha cells, inhibiting apical-basal polarity selectively suppresses beta cell differentiation. Single-cell RNA sequencing and complementary mechanistic data demonstrate that apical-basal polarity in human EPs promotes beta cell specification via cyclic AMP (cAMP)/PKA-cAMP response element binding protein (CREB)-EGR1-mediated inhibition of ARX expression, while reduced cAMP levels in non-polarized human EPs maintain expression of ARX, leading to alpha cell differentiation. These findings identify the apical-basal polarity status of multipotent EPs as a critical epithelial feature that determines their fate into the alpha or beta cell lineages.

## INTRODUCTION

Fate commitment is the sum of unique intrinsic properties and extrinsic cues a progenitor/stem cell receives. While our knowledge of intrinsic properties, such as transcriptional signatures,<sup>1–4</sup> is extensive, much less is known about how fate commitment is regulated by extrinsic cues, such as cell-cell and cell-extracellular matrix (ECM) interactions.<sup>5–8</sup> Discerning the cues that induce cell fate within a dynamically shifting micro-environment constitutes an essential step in understanding organogenesis.

The pancreas is an endoderm-derived glandular organ composed of an exocrine and an endocrine compartment.<sup>9</sup> As pancreas development proceeds, an elaborate tubular network of peripheral tip and central trunk domains forms.<sup>10,11</sup> The tips give rise to acinar cells, whereas the trunk contributes to the duct and endocrine lineages.<sup>12</sup> We have previously demonstrated that differential cell-cell adhesion controls the fate of multipotent pancreatic progenitors by identifying their migration to either the tip or trunk niche, where they are exposed to specific fate-inducing cues.<sup>13</sup> For example, changes in mechanosignaling via actin dynamics instruct the fate of bipotent progenitors into the endocrine and duct lineages within the trunk.<sup>14</sup>

Lineage tracing and loss-of-function experiments prove that all endocrine subtypes, including alpha, beta, delta, epsilon cells, and PP cells, go through an NEUROG3-expressing stage.<sup>15–18</sup> Despite this role of NEUROG3 as the master regulator of the endocrine progenitor (EP) program, the mechanism by which NEUROG3<sup>+</sup> cells give rise to each of the five different endocrine cell types remains undetermined, particularly regarding specifying the fate of the two primary endocrine cell populations, alpha and beta cells. Interestingly, activation of the endocrine program early (embryonic day [E] 8.5) in mouse development, when most of the pancreatic epithelium is non-polarized, almost exclusively yielded alpha cells. In contrast, late (E14.5) endocrine induction, when the progenitor niche consists of a more complex luminal plexus where more EPs have acquired apical-basal polarity, resulted in increased commitment of beta cells.<sup>19–21</sup> Consistently, time-lapse imaging experiments confirmed that beta cells are born as apical-basally polarized epithelial cells.<sup>13,19</sup> Furthermore, forced exiting of NEUROG3<sup>+</sup> cells from the polarized luminal epithelium through conditional ablation of p120ctn or E-cadherin in NEUROG3<sup>+</sup> cells shift their differentiation toward alpha cells at the expense of beta cells.<sup>13</sup> However, far less is known about dynamic changes in the EP niche and the temporal occurrence of hormone cell types during human fetal development.

Drawing upon the aforementioned findings, together with the fact that cadherin-mediated cell-cell adhesion provides essential physical and signaling cues for establishing apical-basal polarity,<sup>22–24</sup> we postulated a connection between cell adhesion and apical-basal cell polarity in influencing the fate determination of NEUROG3<sup>+</sup> cells into the alpha and beta cell lineages. This study demonstrates that dynamic modulation of apical-basal polarity, either directly or indirectly via cell-cell adhesion, within human EPs changes the cell fate preference. While polarized EPs preferentially turn into beta cells via cyclic AMP (cAMP)-mediated inhibition of Aristaless-related homeobox (ARX) expression, non-polarized EPs primarily differentiate into the alpha cell lineage because of failure to increase cAMP levels leading to maintenance of ARX expression.

## RESULTS

### Cell-cell adhesion is linked to apical-basal polarity and cell fate in the human EP niche

To validate the mouse data on the role of cell-cell adhesion for alpha and beta cell specification<sup>13</sup> inside the human EP niche, we generated human embryonic stem cell (hESC) lines that over-express dominant-negative E-cadherin (CDH1) mutants, CDH1ΔE<sup>25</sup> and CDH1ΔP,<sup>26</sup> in a doxycycline (Dox)-inducible manner (Figures 1A and S1A). Overexpression of these mutants, therefore, lowers the adhesive strength between epithelial cells to different degrees.<sup>27</sup> As expected, colonies of CDH1ΔE and CDH1ΔP undifferentiated hESCs lost their epithelial morphology upon Dox treatment and grew as disconnected, spindle-like cells (Figure S1B).

To mimic the *in vivo* epithelial niche of human EPs *in vitro*, we developed a Matrigel overlay culture system based on a previously developed differentiation protocol.<sup>28</sup> In brief, hESCs are seeded in the medium supplemented with Matrigel, which then forms a gelatinous ECM layer covering the cells throughout the subsequent six differentiation stages (S1–S6; Figures S1C and S1D). This allows the cells to efficiently differentiate into a pancreatic endoderm-like epithelium that grows in multiple layers and forms expanding and coalescing luminal cavities with well-defined localized expression of apical-basal polarity markers (Figures S1E and S1F).

The expression of the inducible CDH1 mutant transgenes can be monitored by an internal ribosome entry site (IRES)-coupled mCherry (mCh) fluorescent reporter (Figure S1A). Dox treatment during progressed stages of the differentiation (S4 and later) resulted in a mosaic expression pattern with an average of 40% and 20% expression of mCh in CDH1ΔE and CDH1ΔP cells, respectively (Figures S1G and S1H). We induced dominant-negative E-cadherin overexpression shortly before the first NEUROG3<sup>+</sup> progenitors arise until after the hormone subtypes are specified (S4–S6) and quantified insulin (INS) and glucagon (GCG) expressing cells by flow cytometry. GCG<sup>+</sup>INS<sup>+</sup> polyhormonal cells have previously been shown to mature into alpha cells<sup>29,30</sup> and will, together with GCG<sup>+</sup>INS<sup>-</sup> cells, be referred to as alpha cells, while GCG<sup>-</sup>INS<sup>+</sup> cells are considered to represent beta cells. The differentiating mutant cells only formed very few microlumens that failed to expand into a network of larger connected lumens as observed in the untreated control cultures (Figure 1B). Strikingly, the ratio of beta-to-alpha cells

(beta-to-alpha) was reduced by almost 4-fold in CDH1ΔE- and CDH1ΔP-expressing cells compared with their transgene non-responsive counterparts (Figure 1C). These results strongly suggest that lowered cell-cell adhesion interferes with apical-basal polarity in the human EP niche favoring commitment to an alpha fate over a beta cell fate.

### Disruption of apical-basal polarity in the developing mouse pancreas alters endocrine cell specification

To test whether apical-basal polarity in EPs controls alpha versus beta cell fate *in vivo*, we analyzed conditional *Cdc42* knockout mice. Ablation of the small Rho-family GTPase *Cdc42* in the pancreatic epithelium causes a severe perturbation of apical-basal polarity, lumen expansion, and overall endocrinogenesis.<sup>10</sup> We dissected E16.5 fetal pancreata of *Pdx1-Cre; Cdc42<sup>fl/fl</sup>*; R26-YFP mice (homozygous pancreatic *Cdc42* knockout) and compared them with their *Pdx1-Cre<sup>-</sup>* litter mates as a wild-type control (Figure S2A). More than 95% of the epithelial cells in the knockout expressed yellow fluorescent protein (YFP), indicating a high recombination efficiency (Figure S2B). Consistent with the reported knockout phenotype, only very small microlumens but no tubular network were visible, and the apical membrane-specific marker *Muc1* was abundantly mislocated in intracellular aggregates (Figure S2B).<sup>10</sup> Surprisingly, we found that the number of beta cells was dramatically reduced, while the number of alpha cells remained unchanged in the knockout tissue, resulting in a more than 5-fold reduction in the beta-to-alpha ratio in the *Cdc42* knockout (Figures 1D–1F). In conclusion, disruption of apical-basal polarity in the mouse pancreatic epithelium inhibits beta cell differentiation but does not affect alpha cell differentiation.

### A dynamically changing apical-basal polarity status of human EPs affects alpha versus beta cell fate

Then, we used human fetal pancreas material to examine the apical-basal polarization of EPs. At 9.9 weeks post conception (wpc), we could distinguish roughly equal numbers of polarized and non-polarized EPs in sections stained for NEUROG3 and EZRIN (EZR) (Figure S3A). Furthermore, in our Matrigel overlay hESC model, a plexus-like luminal network, similar to the corresponding luminal network *in vivo*, develops over time from expanding and fusing lumens. Within the 3 days when most EPs are specified (days 10–13; S5), the apical membrane content increases on average by almost 4-fold (Figures 2A and 2B). To quantify the EP polarization status, we utilized a NEUROG3 reporter<sup>19</sup> that allows EP segmentation based on a cytosolic fluorescence signal (enhanced green fluorescent protein [EGFP] under the control of the endogenous NEUROG3 locus; Figure S3B). Due to different protein synthesis and turnover rates, the EGFP and NEUROG3 expression do not entirely overlap in this reporter<sup>31</sup> (Figure 2B). Only EGFP<sup>+</sup> cells that also stained positive for a NEUROG3 antibody were, therefore, segmented and analyzed. Significantly more NEUROG3<sup>+</sup>/EGFP<sup>+</sup> cells featured an apical (EZR<sup>+</sup>) membrane domain on day 13 than on day 10 (Figure 2C). We further analyzed the concomitant lumen expansion and EP appearance by combining the NEUROG3-EGFP reporter with an EZR-mKATE2 fusion reporter (Figure S3C). Long-term (72 h) live-imaging experiments during S5 revealed a highly dynamic epithelial environment in which

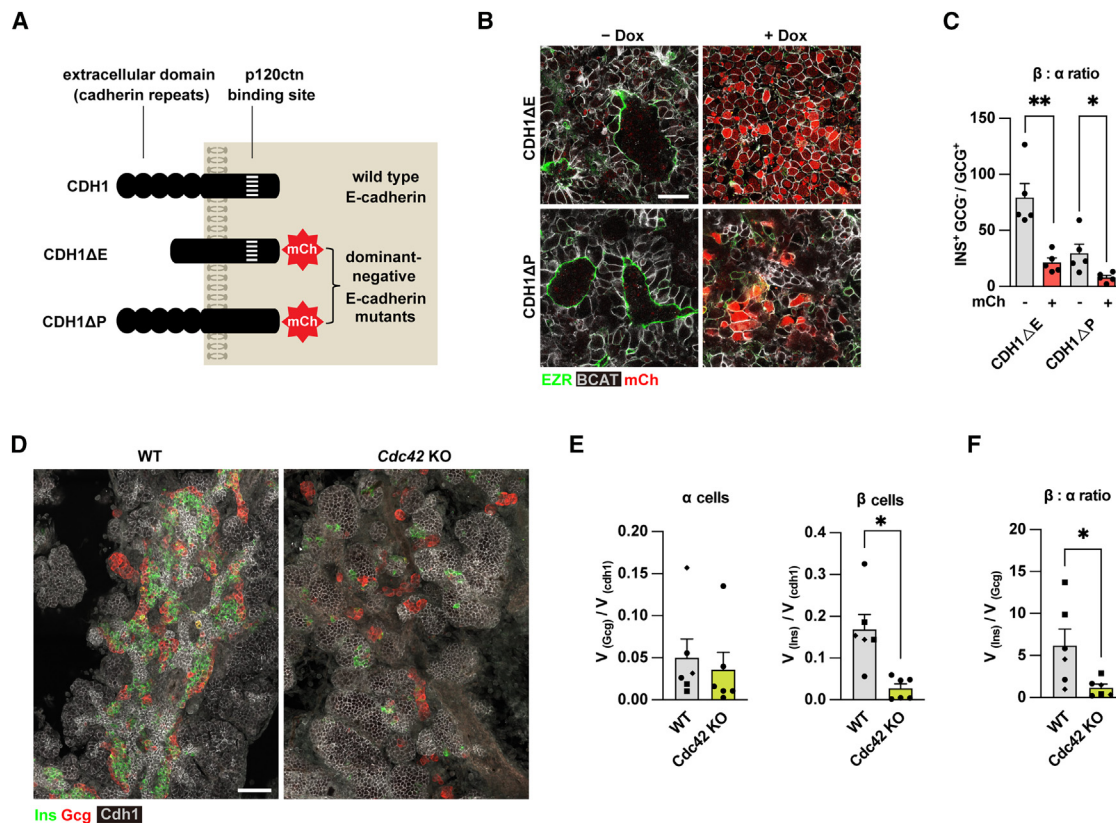


**Figure 1. Disruption of apical-basal polarity by dominant-negative CDH1 mutants in the Matrigel overlay culture system or by *Cdc42* knockout in the developing mouse pancreas alters beta cell specification**

(A) Design of dominant-negative CDH1 mutants with deletions in the extracellular domain (CDH1ΔE) or the p120ctn-binding site (CDH1ΔP). mCh, internal ribosome entry site (IRES)-coupled mCh (red fluorescent protein) reporter.

(B) Confocal images of S5 (day 13) differentiated cells ( $\pm$  72 h Dox treatment). EZR, EZRIN, green; BCAT, beta-catenin, gray; mCh, mCherry, red. Scale bar, 50  $\mu$ m.

(C) Flow cytometry quantification of INS single-positive beta cells and GCG positive alpha cells in mCherry<sup>+</sup> and mCherry<sup>-</sup> subpopulations after Dox treatment (S4–S6). CDH1ΔE and CDH1ΔP mutations led to the same degree of reduction in the INS<sup>+</sup>GCG<sup>-</sup>/GCG<sup>+</sup> ratio in mCherry<sup>+</sup> mutant cells compared with mCherry<sup>-</sup> wild-type cells (4.1-fold reduction in CDH1ΔE and 4.2-fold reduction in CDH1ΔP). Data represent the mean  $\pm$  SD ( $n$  = 5 independent repeats).

(D) Maximum intensity projections (z stack) of confocal tile scans for E16.5 dorsal pancreata stained for INS and GCG expression. INS, green; GCG, red; Cdh1 (E-cadherin), gray. Scale bar, 25  $\mu$ m.

(E) Image quantification based on INS<sup>+</sup> and GCG<sup>+</sup> cell segmentation, normalized to segmented Cdh1<sup>+</sup> epithelial tissue. Data represent the mean  $\pm$  SD ( $n$  = 6 embryos from 3 litters). Different data point symbols indicate different litters.

(F) Image quantification of beta-to-alpha ratio based on segmentation of INS<sup>+</sup> and GCG<sup>+</sup> cells. Data represent the mean  $\pm$  SD ( $n$  = 6 embryos from 3 litters). Different data point symbols indicate different litters.

\* $p$  < 0.05, \*\* $p$  < 0.01 (two-tailed paired Student's  $t$  test).

See also Figures S1 and S2.

the EPs dynamically shifted from being integrated within remodeling lumens and moving around outside the lumens, presumably because of a constant change in their apical-basal polarity status (Video S1).

These results indicate that EPs spend less time in a polarized state before committing to a specific hormone<sup>+</sup> cell type if they arise early during the differentiation. If apical-basal polarization indeed enhances the likelihood for EPs to differentiate into beta cells, one would expect that early-induced EPs give rise to more alpha cells than late-induced EPs. To test this hypothesis directly, we modified the Matrigel overlay differentiation protocol to achieve a more synchronized induction of endocrinogenesis at the earliest time when few EPs normally occur (after the first day of S4). To this end, a set of EP-promoting factors

was added for 2 days (days 8 and 9) to boost early differentiation into EPs, followed by 7 days of culture in basal medium without differentiation factors. A combination of a Notch inhibitor, an ALK5 inhibitor, and the actin polymerization inhibitor latrunculin B<sup>14,28</sup> gave the best results, leading to a wave of NEUROG3 cells that peaked at day 11 and then rapidly subsided (Figures 2D and 2E). For comparison, EP formation was induced the same way 3 days later. Here, we extended the S4 stage to 4 days before adding pro-endocrine factors to limit early EP induction and to allow maturation of the epithelial niche (luminal network) without altering the exposure to other factors. Indeed, a delayed defined EP wave peaking at day 13 was accomplished using this setup (Figures 2D and 2E). We then quantified the resulting alpha and beta cells from the early and late EP protocols by flow cytometry.

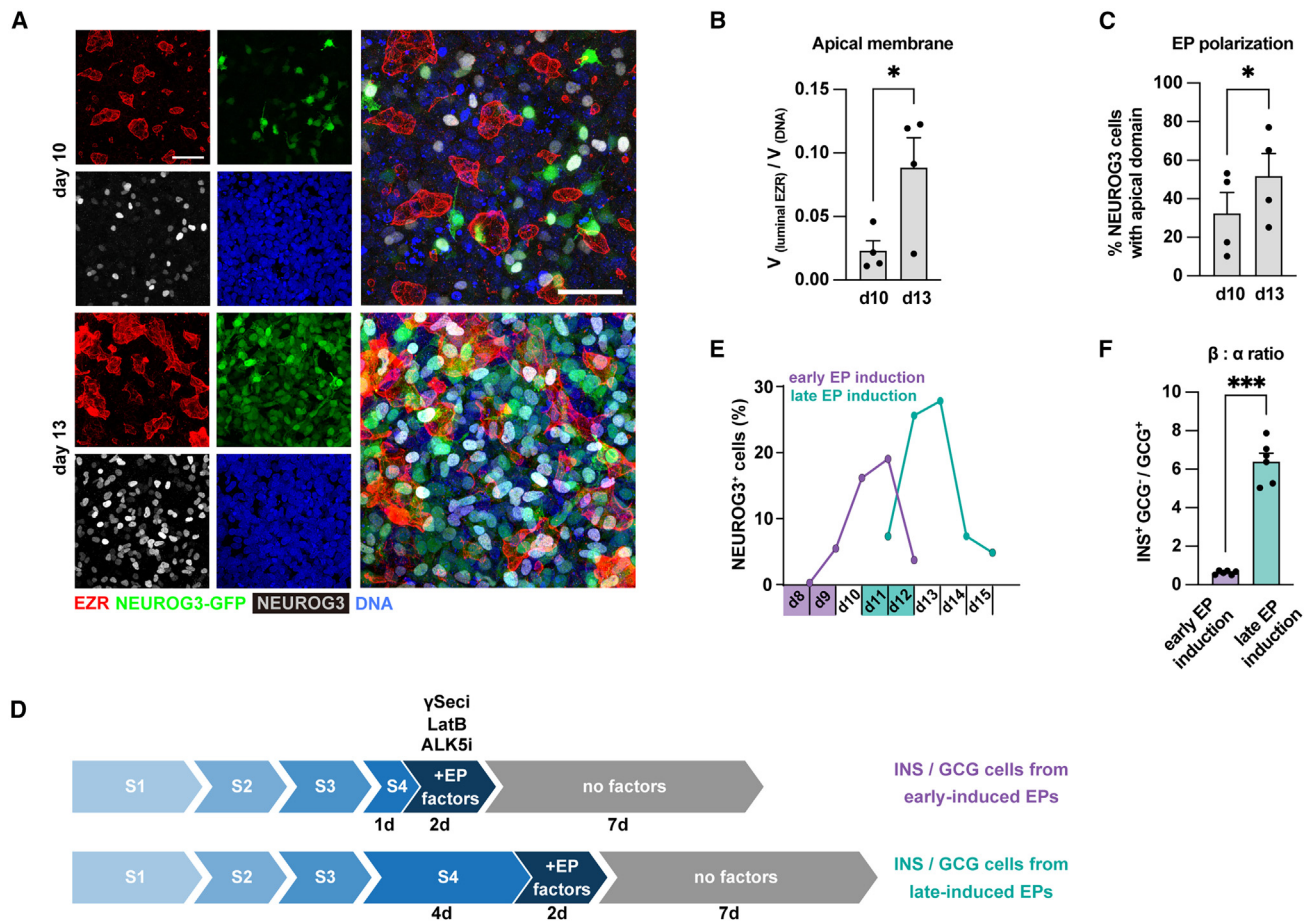


**Figure 2. Apical-basal polarity in the human EP niche affects alpha versus beta cell fate**

(A) Luminal network development and EP generation in S5 differentiating cultures. Images show maximum intensity projections of confocal z stacks. EZR, red; NEUROG3-EGFP, green; NEUROG3 (antibody staining), gray; DNA (DAPI), blue. Scale bar, 50  $\mu\text{m}$ .

(B) Image quantification of apical membrane content is based on the segmentation of the luminal EZR signal, normalized to DNA content. In detail, the surface module of the Imaris image analysis software (Oxford Instruments) was used to render a 3D segmentation of the luminal/apical EZR signal. The volume of the segmented structures ( $V_{\text{luminal EZR}}$ ) was quantified and divided by the volume of the DNA (DAPI) signal ( $V_{\text{DNA}}$ ) to normalize for differences in cell numbers between different images. “Volume” in this context refers to the sum of voxels of the EZR segmentation (representing a quantification of the apical membranes). Data represent the mean  $\pm$  SEM ( $n = 4$  independent repeats).

(C) Image quantification of apical-basally polarized EPs. The percentage of NEUROG3<sup>+</sup> cells (identified by NEUROG3-EGFP<sup>+</sup> and nuclear NEUROG3<sup>+</sup>) containing EZR<sup>+</sup> membranes is shown. Data represent the mean  $\pm$  SEM ( $n = 4$  independent repeats).

(D) Experimental setup for assessing the differentiation potential of early- and late-induced EPs. EP factors were treated on day 8 (early-induced) or day 11 (late-induced) for 2 days. LatB, latrunculin B.

(E) Flow cytometry quantification of synchronized endocrinogenesis. The periods of treatment with pro-endocrine factors and the percentage of NEUROG3<sup>+</sup> cells are indicated.

(F) Flow cytometry quantification of the beta-to-alpha ratio after early or late EP induction. Data represent the mean  $\pm$  SEM ( $n = 6$  independent repeats).

\* $p < 0.05$ , \*\*\* $p < 0.001$  (two-tailed paired Student’s t test).

See also [Figure S3](#) and [Video S1](#).

Strikingly, the beta-to-alpha ratio was, on average, more than 10-fold higher in hormone cell populations derived from EPs that originated in a more mature environment characterized by a more apical-basally polarized epithelium ([Figure 2F](#)).

### Apical-basally polarized human EPs are primed to become beta cells

Next, we set out to test more directly whether alpha and beta cell fate depends on the apical-basal polarity status of EPs by a cell sorting approach. Prominin-1 (PROM1, CD133) was identified as

a specific marker of apical membranes/lumens in the Matrigel overlay culture system ([Figure 3A](#)). Moreover, PROM1 is exclusively expressed in apical membrane domains and co-localizes with other apical markers (MUC1, EZR, and aPKC) in 10.6 wpc human fetal pancreas tissue ([Figures S3D](#) and [S3E](#)). PROM1 is a highly evolutionary conserved transmembrane glycoprotein located within the apical microvilli of embryonic and adult mammalian epithelial cells. Importantly, it contains two large extracellular loops, rendering it a potential marker for antibody-based cell sorting for apical-basally polarized cells.<sup>32</sup>

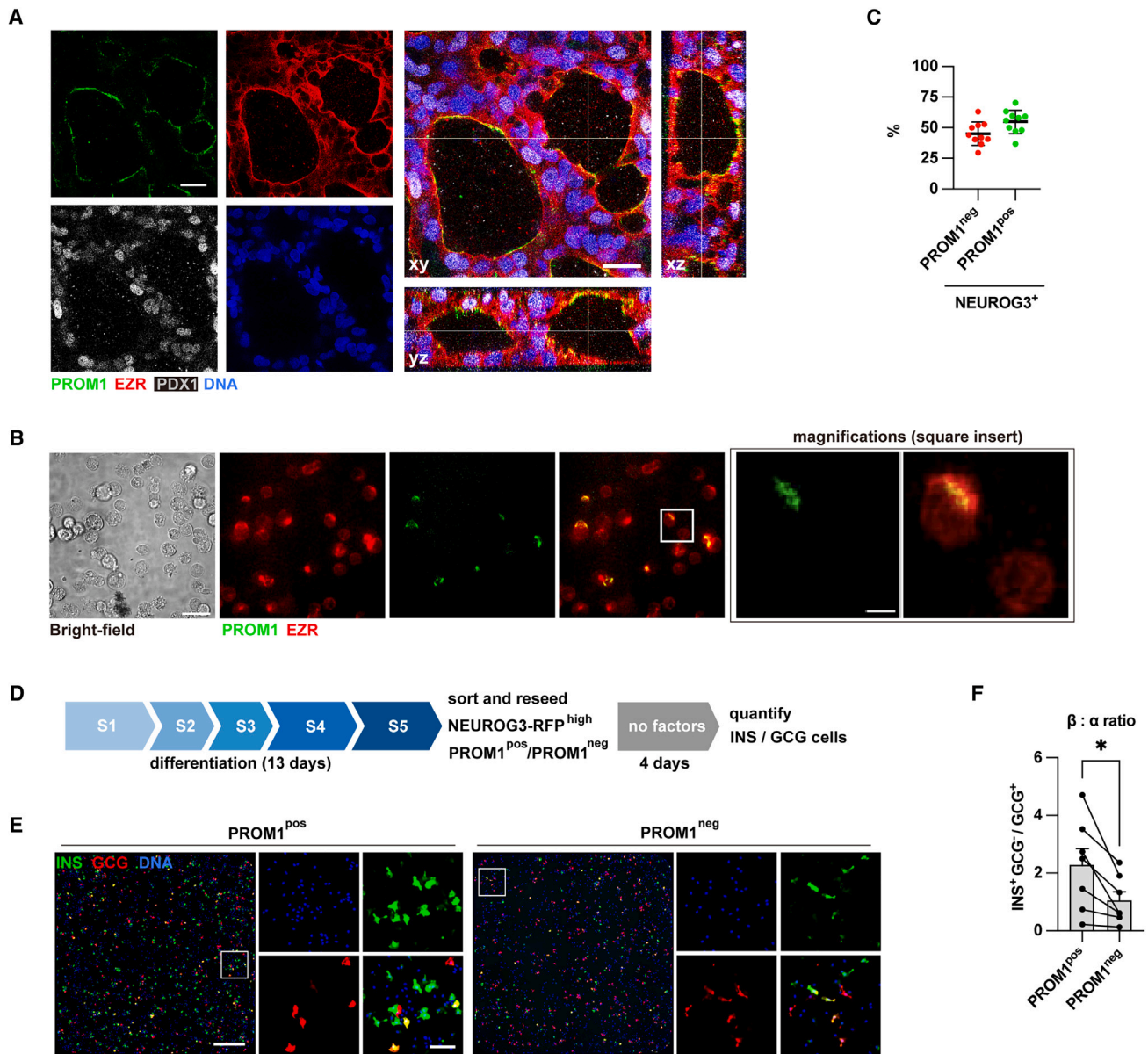


**Figure 3. Apical-basally polarized human EPs are primed to become beta cells**

(A) Apical membrane-specific localization of PROM1 in S5 (day 13) differentiating cultures. PROM1, CD133, green; EZR, red; PDX1, gray; DNA (DAPI), blue. Scale bar, 25  $\mu$ m.

(B) A subset of cells in S5 differentiating cultures retain a PROM1<sup>+</sup> membrane domain (green) after dissociation. Phase-contrast image and magnifications (square insert) show dissociated S5 cells. EZR (red) is expressed in all cells but is enriched in the apical domain. Scale bar, 25 and 5  $\mu$ m (magnifications and square insert, respectively).

(C) Flow cytometry quantification of the percentage of PROM1<sup>-</sup> and PROM1<sup>+</sup> cells in NEUROG3<sup>+</sup> cell population at S5 (day 13). Data represent the mean  $\pm$  SD ( $n = 10$  independent repeats).

(D) Experimental setup for assessing the differentiation potential of polarized and non-polarized EPs by flow cytometry sorting. S5 (day 13) cells are dissociated and sorted by NEUROG3-TagRFPT and PROM1. The sorted TagRFPT<sup>+</sup>PROM1<sup>-</sup> and TagRFPT<sup>+</sup>PROM1<sup>+</sup> cells were reseeded in 2D and cultured for 4 days with basal medium.

(E) Immunocytochemistry for INS and GCG expression in sorted and reseeded PROM1<sup>+</sup> and PROM1<sup>-</sup> EPs after 4 days of culture. Confocal tile scans and magnifications (square insert). INS, red; GCG, green; DNA (DAPI), blue. Scale bars, 500  $\mu$ m (left)/100  $\mu$ m (insert, right).

(F) Imaging-based quantification of the beta-to-alpha ratio after sorting EPs for PROM1. Data represent the mean  $\pm$  SEM ( $n = 7$  independent repeats).

\* $p < 0.05$  (two-tailed paired Student's  $t$  test).

See also [Figure S3](#).

Interestingly, a subset of dissociated S5 cells stained with a PROM1 antibody featured a cap-like PROM1<sup>+</sup> structure on one side of the cell. This PROM1<sup>+</sup> membrane area was also enriched in EZR, suggesting that it represents the remnant of the apical domain in previously polarized cells (Figure 3B). In contrast, other cells showed no PROM1 staining and homogeneous membrane and intracellular EZR distribution, presumably representing previously non-polarized cells (Figure 3B). This observation is consistent with the finding that polarization can be sustained by single cells in suspension.<sup>33</sup> Furthermore, PROM1<sup>+</sup> and PROM1<sup>-</sup> cell populations could be separated from S5 Matrigel overlay differentiation cultures by flow cytometry. To specifically sort EPs based on their apical-basal polarization status (PROM1<sup>+</sup>/PROM1<sup>-</sup>), we took advantage of a NEUROG3-TagRFPt fusion reporter<sup>34</sup> (Figure S3F). At S5, the NEUROG3-TagRFPt<sup>+</sup> cell population contained around 45.13% PROM1<sup>-</sup> and 54.87% PROM1<sup>+</sup> cells (Figure 3C).

After completion of the EP stage (S5), Matrigel overlay-differentiated NEUROG3<sup>high</sup> cells were sorted for membranous PROM1 expression, reseeded at low density onto Matrigel-coated surfaces, and allowed to differentiate for an additional 4 days without any specific factors (Figure 3D). These cultures were then stained for INS and GCG expression and quantified by image analysis (Figure 4E). The beta-to-alpha ratio was more than twice as high in hormone<sup>+</sup> cell populations derived from PROM1<sup>+</sup> EPs than in those derived from PROM1<sup>-</sup> EPs (Figure 3F), suggesting that EPs that were polarized at the time of sorting are predisposed to adopt a beta cell fate.

### scRNA-seq reveals differentiation propensities in polarized EPs

To gain further insight into the link between the apical-basal polarity status of EPs and fate allocation, we conducted single-cell RNA sequencing (scRNA-seq) of early-induced EPs, late-induced EPs, PROM1<sup>-</sup> late-induced non-polarized EPs, and PROM1<sup>+</sup> late-induced polarized EPs (Figure 4A). We then labeled these samples with four different antibodies conjugated to barcoded oligonucleotides (“hashtags”) before pooling and sequencing all samples together (Figure 4A).

This cellular indexing of transcriptomes and epitopes by sequencing (CITE-seq)<sup>35</sup> allowed us to allocate each single-cell transcription profile to the cell’s original characteristics (apical-basal polarization and time of endocrine induction). After quality filtering for viability parameters and normalization, we obtained transcriptional data from 3,811 cells, including counts for 25,917 genes. Based on clustering and marker gene expression (Figures S4A and S4B), we identified populations of bipotent pancreatic progenitors, ductal cells, pancreatic stellate cell (PSC)-like cells, as well as a big supercluster corresponding to cells of the endocrine lineage. Most of the latter expressed the EP-state marker NEUROG3 and pan-endocrine genes like NEUROD1, NKX2-2, and CHGA. While a subset of cells also expressed markers of early hormone<sup>+</sup> cells such as MAFB and INS, markers of more mature hormone<sup>+</sup> cells such as MAFA were absent (Figure S4B). These signatures suggest that, as intended, we captured different EP stages, including both unspecified progenitors and cells that have already committed to specific endocrine subtypes. Moreover, we identified 3,281 cells (86%) labeled with a single hashtag, with a roughly equal contribution by the four

barcodes (Figure S4C). Hashtag-negative and double-labeled cells/doublets were excluded from all subsequent analyses.

Sub-clustering of the endocrine cell population yielded 12 distinguishable populations (Figure 4B). The transcriptional profiles (Figures S4D and S4E) and pseudo-time analysis (Figure S4F) suggest that clusters 9 and 11 contain unspecified early-state EPs. The clusters 8 (“pre-alpha 1”) and 12 (“pre-alpha 2”) have increasingly specific alpha-like signatures, whereas clusters 2, 3, 1 (“pre-beta 1”), and 10 (“pre-beta 2”) appear to represent a distinct differentiation trajectory leading to beta-like transcriptional profiles. Cluster 7 comprises endocrine cells committed to the delta lineage (“pre-delta”).

Next, we analyzed the distribution of the four hashtags throughout the endocrine population (Figures 4C and 4D). The same number of endocrine cells originated from early and late induction cultures. Early-induced EPs mainly contributed to clusters 4, 5, and 9, as well as clusters pre-alpha 1 and pre-delta. While late-induced EPs contributed to all clusters, the pre-beta 1 and pre-beta 2 clusters were almost exclusively comprised of late-induced cells. Most of all endocrine cells were non-polarized. Polarized endocrine cells were mostly confined to fate-specified clusters. The pre-beta 1 and pre-beta 2 clusters contained significantly more polarized cells (52% and 89%, respectively) than the pre-alpha 1, pre-alpha 2, and pre-delta clusters (4%, 33%, and 23%, respectively).

We directly compared the transcriptional profiles between early- and late-induced and between non-polarized and polarized endocrine cells and observed an overlap with genes associated with beta cell differentiation in the late-induced and polarized EP signatures (e.g., *DLK1*, *CHGA*, and *INS*) (Figure 4E). The top differentially expressed genes in early-induced versus late-induced and non-polarized versus polarized endocrine cells were validated by quantitative real-time PCR analysis (Figure S4G). Among these genes, *DLK1*, a non-canonical Notch ligand, is considered a beta-lineage-specific marker and is more highly expressed in beta cells compared with other pancreatic endocrine cell types.<sup>36</sup> However, knockdown of *DLK1* in EPs using small interfering RNA (siRNA) did not alter the differentiation into alpha or beta cells (Figures S4H and S4I), suggesting that *DLK1* is not involved in determining beta cell fate. Additionally, Sox4 has been shown to regulate endocrine pancreas formation cooperatively with Neurog3, but there is no evidence to suggest that SOX4 is involved in the human alpha and beta cell fate choice.<sup>37,38</sup>

In conclusion, the CITE-seq data indicate that most alpha cells are generated from non-polarized EPs (either early or late-induced), while beta cells arise predominantly from late-induced, polarized EPs.

### Apical-basal polarity promotes beta cell fate by suppressing ARX expression

To identify potential candidate genes relevant for alpha versus beta cell fate allocation, we filtered our CITE-seq data of non-polarized versus polarized EPs with previously published pre-beta and pre-alpha scRNA-seq data (Table S3).<sup>39</sup> This analysis revealed ten genes that were consistently upregulated in polarized EPs and early beta cells (*DLK1*, *CRYBA2*, *TAGLN2*, *SCGN*, *FABP7*, *TSPAN1*, *AIF1*, *PAM*, *CHGA*, and *SLC8A8*) and two genes that were consistently upregulated in non-polarized

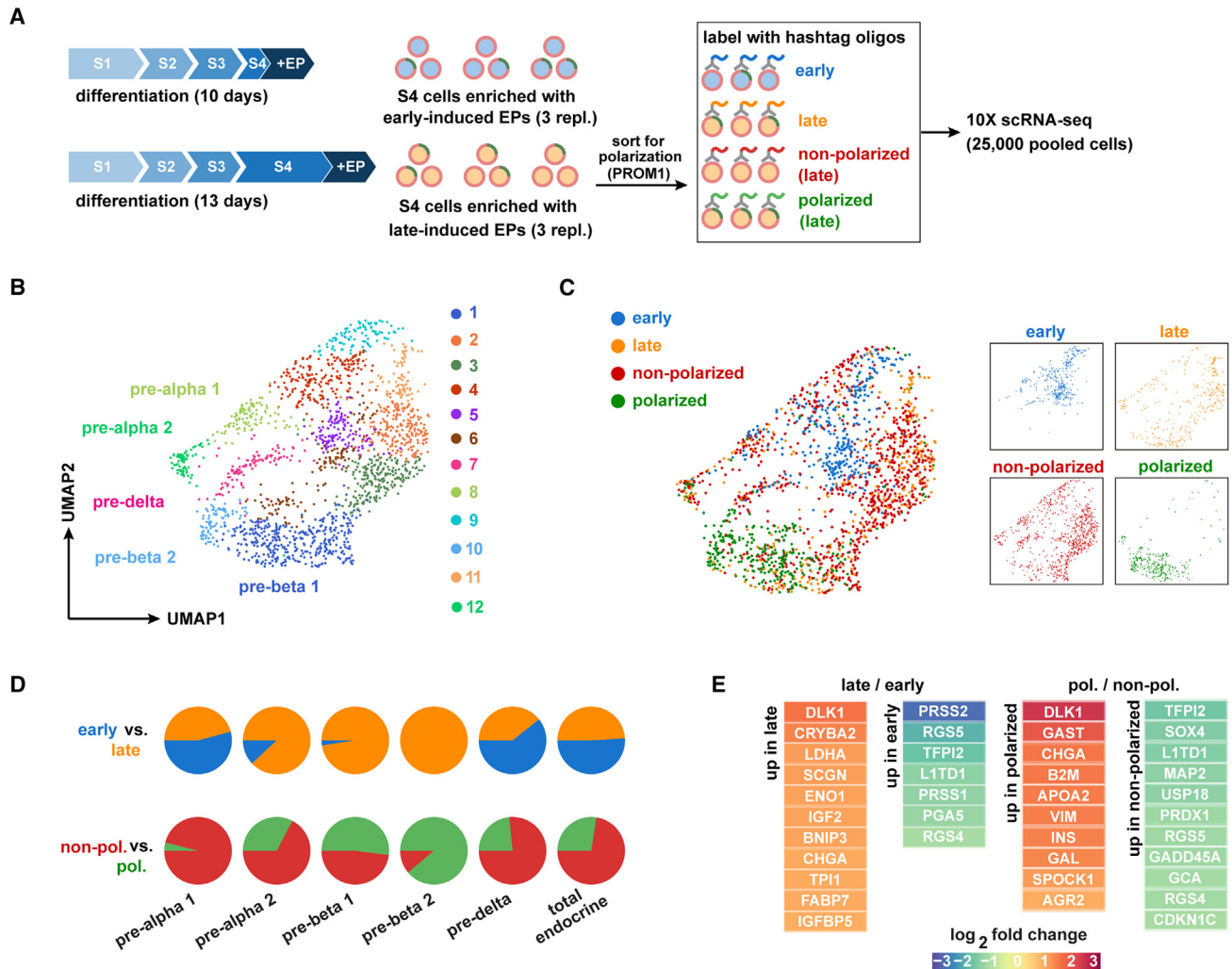


**Figure 4. scRNA-seq reveals differentiation propensities in polarized EPs**

(A) Setup of the CITE-seq experiment to investigate different types of EPs by hashtag conjugation. All cells were sorted for single, living (DAPI<sup>-</sup>) cells before treatment with hashtag antibodies. Late-induced cell cultures were additionally sorted for apical-basal polarity (PROM1<sup>-</sup>, non-polarized; PROM1<sup>+</sup>, polarized). Each sample consists of three biological replicates.

(B) Clustering uniform manifold approximation and projection (UMAPs) showing 12 endocrine subclusters in all four samples.

(C) Allocation of hashtags to individual cells and subclusters. Early-induced EPs, blue; late-induced EPs, orange; late-induced non-polarized EPs, red; late-induced polarized EPs, green.

(D) Comparison of fraction of cells labeled with hashtags for early/late EP induction and non-polarized/polarized status in selected subclusters.

(E) Enriched transcripts upon the comparison between early- and late-induced and between non-polarized and polarized endocrine cells (log<sub>2</sub> fold change > 1, adjusted *p* value < 0.0001).

See also Figure S4.

EPs and early alpha cells (ARX and C7) (Figure 5A). Notably, ARX is a downstream target of NEUROG3 and has been previously demonstrated to regulate the generation of alpha cells.<sup>40</sup> In line with previous findings, we confirmed the absence of ARX expression in early EPs (NEUROG3-TagRFPt<sup>+</sup>EGFP<sup>-</sup>) by immunocytochemistry, contrasting with its later expression (NEUROG3-TagRFPt<sup>+</sup>EGFP<sup>+</sup> and NEUROG3-TagRFPtEGFP<sup>+</sup>) (Figures S5A and 5B). Additionally, quantitative real-time PCR data show that ARX expression precedes GCG expression (Figure S5C). Both immunofluorescence and flow cytometry analyses reveal a nearly complete overlap between GCG<sup>+</sup> cells

and ARX<sup>+</sup> cells (Figures S5D and 5E). Taken together, these findings suggest that ARX, as a downstream component of NEUROG3, may influence the fate determination of alpha cells (Figure S5F). In alignment with the scRNA-seq data, RT-qPCR and western blot analysis confirmed elevated expression of ARX in PROM1<sup>-</sup> EPs compared with PROM1<sup>+</sup> EPs (Figures 5B and 5C). Moreover, flow cytometry analysis showed that PROM1<sup>-</sup> cells exhibited a higher proportion of ARX<sup>+</sup> cells when compared with PROM1<sup>+</sup> cells (Figure 5D). Collectively, these findings suggest that a non-polarized status of EPs maintains ARX expression.

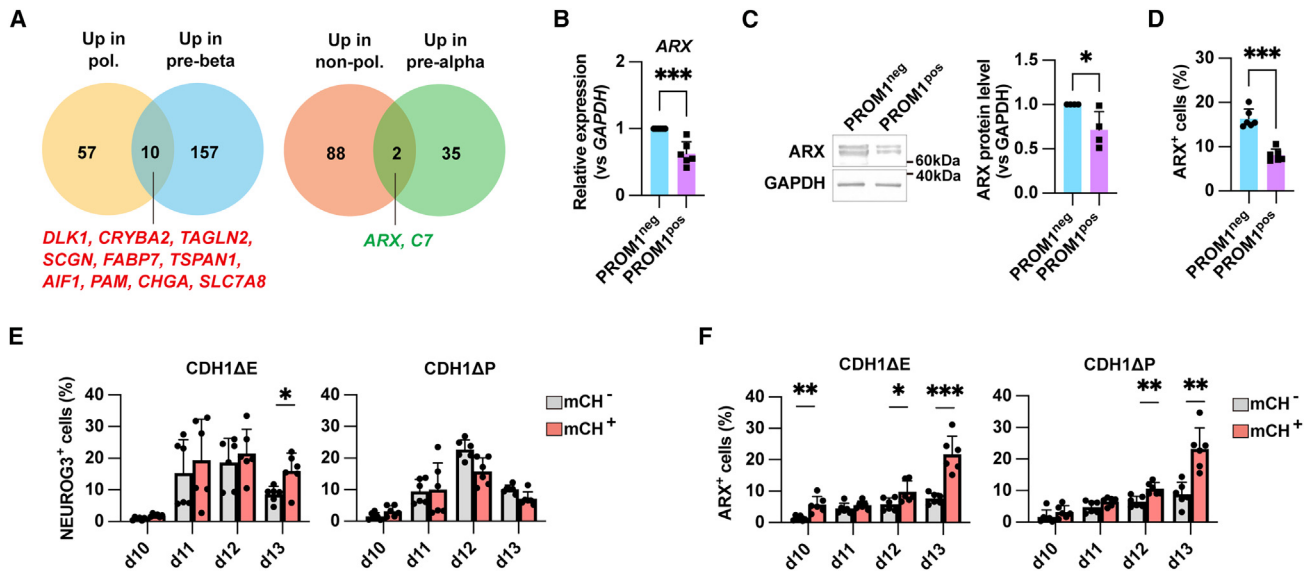


**Figure 5. Apical-basal polarity promotes beta cell fate by suppressing ARX expression**

(A) Venn plots showing overlaps of enriched genes between polarized EPs (versus non-polarized EPs) and early beta cells (versus early alpha cells), as well as of enriched genes between non-polarized EPs (versus polarized EPs) and early alpha cells (versus early beta cells). The scRNA-seq data from pre-beta cells versus pre-alpha cells were obtained from a published dataset.<sup>39</sup>

(B and C) Validation of differential ARX expression between TagRFP<sup>+</sup>PROM1<sup>-</sup> and TagRFP<sup>+</sup>PROM1<sup>+</sup> cells at day 13 by quantitative real-time PCR (B) and western blot (C). GAPDH served as a loading control. Data represent the mean  $\pm$  SD ( $n = 6$  for quantitative real-time PCR;  $n = 4$  for western blot, independent repeats).

(D) Flow cytometry quantification of the percentage of ARX<sup>+</sup>PROM1<sup>-</sup> and ARX<sup>+</sup>PROM1<sup>+</sup> cells in S5 (day 13) differentiating Matrigel overlay cultures. Data represent the mean  $\pm$  SD ( $n = 6$  independent repeats).

(E and F) Flow cytometry quantification of the percentage of NEUROG3<sup>+</sup> cells (E) and ARX<sup>+</sup> cells (F) between mCherry<sup>+</sup> and mCherry<sup>-</sup> subpopulations during days 10–13 after Dox treatment. Data represent the mean  $\pm$  SD ( $n = 6$  independent repeats).

\* $p < 0.05$ , \*\* $p < 0.01$ , \*\*\* $p < 0.001$  (two-tailed paired Student's  $t$  test).

See also [Figures S5](#) and [S6](#) and [Tables S2](#) and [S3](#).

To further validate these findings, we utilized our previous observation that inhibition of cadherin function in EPs interferes with apical-basal polarity promoting alpha cell differentiation (Figure 1C). The ratio of NEUROG3<sup>+</sup> cells was not significantly different between CDH1ΔE and CDH1ΔP expressing (mCherry<sup>+</sup>) cells and mCherry<sup>-</sup> control cells (Figure 5E) except for day 13 CDH1ΔE cultures, indicating that CDH1 mutations do not affect EP generation. However, the ratio of ARX<sup>+</sup> cells was higher in CDH1ΔE and CDH1ΔP mCherry<sup>+</sup> cells compared with mCherry<sup>-</sup> cells on S5 (days 12 and 13), demonstrating that CDH1 mutations increase ARX expression (Figure 5F).

### Apical-basal polarity regulates ARX expression via cAMP signaling

To further explore how apical-basal polarity regulates ARX expression, we performed an *in silico* transcription factor (TF) motif analysis<sup>41,42</sup> of the ARX locus to predict which TFs can bind within 2 kb of the transcriptional start site of ARX (Table S2). The only TF with a binding motif in this region of the ARX locus that was differentially expressed in polarized versus non-polarized EPs was Early growth response 1 (EGR1) (Tables S2 and S3). Consistent with the scRNA-seq data, we detected an elevated expression of EGR1 in PROM1<sup>+</sup> EPs compared with PROM1<sup>-</sup> EPs by quantitative real-time PCR and western blot analyses (Figures 6A and 6B). EGR1 has been shown to bind to *Pdx1* and *Arx* in mice, positively regulating

*Pdx1* while negatively regulating *Arx* expression. Moreover, high-fat-fed *Egr1*<sup>-/-</sup> mice exhibit decreased beta cell and increased alpha cell numbers.<sup>43</sup> To test whether EGR1 expression is linked to alpha and beta cell fate choice, we knocked down EGR1 expression in S5 cells using siRNAs. Based on the quantitative real-time PCR results, we confirm that EGR1 negatively regulates ARX expression (Figure 6C). Furthermore, we observed a decreased beta-to-alpha cell ratio in EGR1 knockdown (EGR1-siRNA) cells compared with the negative-siRNA (NEG-siRNA) control group (Figure 6D).

The cAMP/protein kinase A (PKA)-cAMP-response-element-binding protein (CREB) signaling pathway can enhance EGR-1 gene transcription.<sup>44</sup> By ELISA analysis, we found cAMP levels to be higher in PROM1<sup>+</sup> polarized EPs compared with PROM1<sup>-</sup> non-polarized EPs (Figure 6E). To more directly test whether increased cAMP activity promotes beta cell differentiation, we treated EP-stage cells (S5, days 10–13) with the cAMP agonists forskolin (FSK, an adenylate cyclase activator) and 3-isobutyl-1-methylxanthin (IBMX, a competitive non-selective phosphodiesterase inhibitor), separately. Although cocktails of FSK together with other small molecules/growth factors have been used to boost differentiation of beta cells,<sup>45–47</sup> no data on its mechanism of action have been provided. FSK treatment led to a pronounced and transient elevation in the phosphorylation of CREB, peaking within 1–2 h (Figure 6F). Consistently, the expression level of EGR1 also exhibited a pronounced and

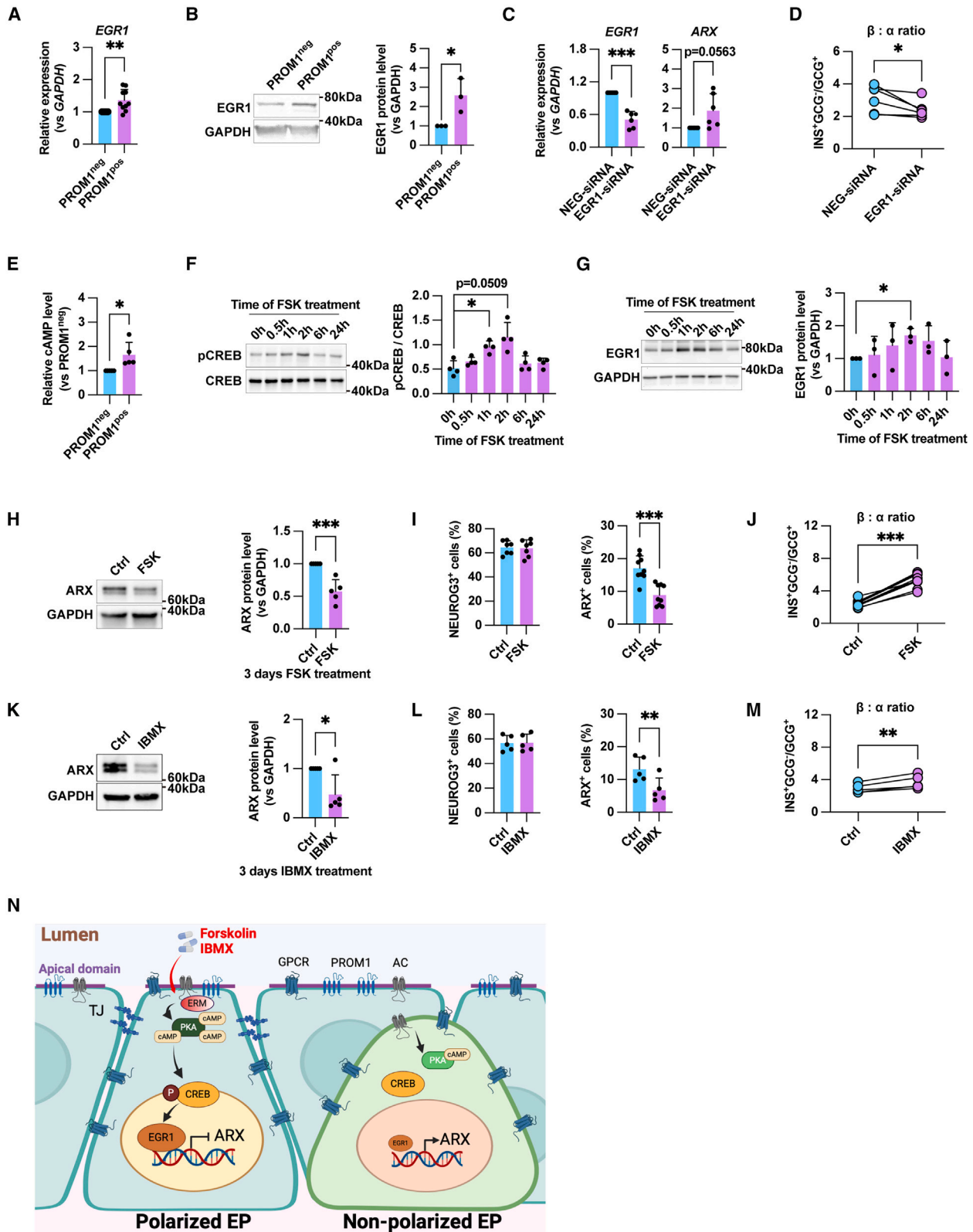


**Figure 6. Apical-basal polarity regulates ARX expression via cAMP signaling**

(A and B) Quantification of EGR1 expression in PROM1<sup>-</sup> and PROM1<sup>+</sup> EPs at day 13 by RT-qPCR (A) and western blot (B). GAPDH served as a loading control ( $n = 10$  for quantitative real-time PCR;  $n = 3$  for western blot, independent repeats).

(legend continued on next page)

transient increase, reaching its maximum at 2 h (Figure 6G). Conversely, the expression level of ARX decreased after 3 days of FSK treatment (Figure 6H). Importantly, while FSK treatment did not alter the proportion of NEUROG3-GFP<sup>+</sup> endocrine cells, it significantly reduced the fraction of ARX<sup>+</sup> cells (Figure 6I), resulting in an elevated beta-to-alpha ratio (Figure 6J). Consistently, IBMX treatment yielded comparable results to FSK treatment in reducing ARX expression and increasing the beta-to-alpha ratio (Figures 6K–6M). Thus, our data not only identify apical-basal polarity as the epithelial feature that controls the specification of EPs into alpha and beta cells but also explain how.

## DISCUSSION

In early mammalian embryo development, apical-basal polarity plays a critical role in the initial lineage allocation between inner cell mass and trophectoderm. By the end of the 8-cell stage, the outer cells of embryos acquire apical-basal polarity, which promotes Yap nuclear localization, leading to the expression of Cdx2 and the commitment to the trophectoderm lineage.<sup>48–50</sup> During organogenesis, multipotent epithelial progenitors coordinate tissue remodeling and fate decisions, and compelling evidence exists for a reciprocal governance relationship between these processes. While it is known that apical-basal polarity governs the balance between proliferation and differentiation of neural progenitors through Notch signaling,<sup>51–54</sup> it remains unclear whether apical-basal polarity controls subsequent fate decisions of multipotent neural progenitors. The dynamic nature of tissue remodeling implies that epithelial features, such as apical-basal polarity, continuously change. Therefore, a fundamental question is how dynamic changes

in multipotent epithelial progenitor features directly affect their cell lineage decisions.

In this study, we identified a direct role of apical-basal polarity in the fate allocation of EPs into the beta and alpha cell lineages. Specifically, we demonstrate that apical-basal polarity in EPs promotes beta cell specification via cAMP/PKA-CREB-EGR1-mediated inhibition of ARX expression, while reduced cAMP levels in non-polarized EPs maintain expression of ARX leading to alpha cell differentiation.

In mice, Pax4 promotes the formation of beta cells by inhibiting Arx.<sup>40</sup> However, while PAX4 plays a role in regulating human beta cell function, it is not crucial for beta cell specification.<sup>55</sup> While depletion of ARX in mouse and human (hESCs) leads to the removal of alpha cells,<sup>40,55</sup> the beta cell number increases in mouse but decreases in human.<sup>40,56,57</sup> Importantly, temporary rescue of ARX expression in ARX-knockout pancreatic progenitors restores the specification of beta cells but not alpha cells, suggesting that sustained ARX expression is vital for alpha cell formation.<sup>56</sup>

The key link between the cAMP/PKA-CREB signaling pathway and the transcriptional machinery involved in beta and alpha cell specification is mediated by EGR-1 and ARX. We identified EGR-1 as a negative regulator of ARX expression. EGR-1 gene transcription is regulated by G-protein-coupled receptors (GPCRs) via the cAMP/PKA-CREB signaling pathway in pancreatic beta cells.<sup>44</sup> However, none of the GPCRs expressed in EPs are differentially expressed in polarized versus non-polarized EPs. Another potential regulator of this pathway is PROM1. First, PROM1 is specifically expressed in polarized EPs (Figures 3A, S3D, and S3E). Second, Prom1 regulates hepatic gluconeogenesis and adipogenesis via membrane recruitment of EZR-Radixin-Moesin (ERM) family proteins, thereby bringing PKA in close proximity to GPCRs, adenylyl cyclase (AC), and PKA substrates

(C) Validation of *EGR1* and *ARX* expression by quantitative real-time PCR in NEG-siRNA and *EGR1*-siRNA cultures. Data represent the mean  $\pm$  SD ( $n = 6$  independent repeats).

(D) Flow cytometry quantification of the beta-to-alpha ratio in NEG-siRNA and *EGR1*-siRNA cultures on day 17. Data represent the individual biological repeats ( $n = 6$  independent repeats).

(E) ELISA quantification of cAMP level in PROM1<sup>-</sup> and PROM1<sup>+</sup> EPs at day 13. Data represent the mean  $\pm$  SD ( $n = 5$  independent repeats).

(F and G) Western blot quantification of phosphorylated CREB (pCREB) (F) and *EGR1* (G) protein levels after 0, 0.5, 1, 2, 6, and 24 h 10  $\mu$ M FSK treatment. Data represent the mean  $\pm$  SD ( $n = 4$  for pCREB;  $n = 3$  for *EGR1*, independent repeats).

(H) Western blot quantification of ARX protein levels in control and FSK treatment cells at S5 (day 13). FSK was treated from days 10 to 13. GAPDH served as a loading control. Data represent the mean  $\pm$  SD ( $n = 5$  independent repeats).

(I) Flow cytometry quantification of the NEUROG3-EGFP<sup>+</sup> (represents the whole endocrine cells) and ARX<sup>+</sup> proportion in control and FSK-treated cells at day 13. (NEUROG3:  $n = 7$ ; ARX:  $n = 9$ , independent repeats).

(J) Flow cytometry quantification of the beta-to-alpha ratio in control and FSK-treated cultures on day 17. Data represent the individual biological repeats ( $n = 9$ , independent repeats).

(K) Western blot quantification of ARX protein levels in control and IBMX treatment cells at S5 (day 13). IBMX was treated from days 10 to 13. GAPDH served as a loading control. Data represent the mean  $\pm$  SD ( $n = 5$ , independent repeats).

(L) Flow cytometry quantification of the NEUROG3-EGFP<sup>+</sup> (represents the whole endocrine cells) and ARX<sup>+</sup> proportion in control and IBMX-treated cells on day 13. Data represent the mean  $\pm$  SD ( $n = 5$ , independent repeats).

(M) Flow cytometry quantification of the beta-to-alpha ratio in control and IBMX-treated cultures on day 17. Data represent the individual biological repeats ( $n = 5$ , independent repeats).

(N) Model illustrating the proposed mechanism for regulation of pancreatic beta and alpha cell allocation by apical-basal polarity. Tight junctions (TJs) provide essential physical and signaling cues for establishing apical-basal polarity. Within the polarized EPs, PROM1 facilitates the recruitment of ERM family proteins to bring PKA to membrane lipid rafts where GPCR, AC, and PKA substrates are in close proximity to increase the response of cAMP signals. The resulting increased activity of cAMP/PKA-CREB signaling promotes the expression of *EGR1* and further inhibits the expression of *ARX*, thereby allowing EPs to differentiate into beta cells. In the non-polarized environment, EPs exhibit relatively low activity of cAMP/PKA-CREB signaling, subsequently diminishing *EGR1* expression and permitting the expression of *ARX*. This shift allows EPs to differentiate into alpha cells. FSK and IBMX, as cAMP agonists, can increase intracellular cAMP levels and promote the generation of beta cells.

\* $p < 0.05$ , \*\* $p < 0.01$ , \*\*\* $p < 0.001$  (two-tailed paired Student's *t* test).

See also Figure S6.

within membrane lipid rafts.<sup>58,59</sup> The fact that PROM1 and EZR are specifically localized at the apical membrane of polarized EPs (Figures 3A and S3E) suggests a similar role of PROM1 in the regulation of the cAMP/PKA-CREB signaling pathway in polarized EPs.

Considering the dynamic shift of EPs between polarized and non-polarized states and the short half-life of cAMP, we speculate that only when apical-basal polarity stabilizes will PROM1/EZR proteins be able to bring all the components of the cAMP/PKA-CREB signaling pathway in proximity on the apical membrane. This enables activation of the pathway to ultimately induce beta cell specification via reduced expression of ARX. In such a scenario, the reason that some polarized (PROM1<sup>+</sup>) EPs do not differentiate into INS<sup>+</sup>GCG<sup>-</sup> cells may be due to an insufficient accumulated time in a polarized state or failure to acquire a mature state of apical-basal polarity.

Our findings emphasize the importance of temporal analysis of the microenvironment of multipotent progenitors, including their cell biological features, to identify the unique signal for each fate-inducing event. We therefore expect that dynamic analysis of multipotent progenitors in other organs, such as the lung, brain, and mammary gland, is likely to be of great help in identifying the fate-inducing extrinsic cues in respective organs.

### Limitations of the study

While we have demonstrated that EPs retain their apical-basal polarity following cell dissociation, it is important to acknowledge that the processes of cell dissociation and sorting may alter the original status of the cells. These changes may introduce artifacts or variability that could impact the outcomes of the CITE-seq analysis. However, functional validation of the CITE-seq data eliminated the risk that the differentially expressed genes in polarized and non-polarized EPs were irrelevant. In addition, although we have established a role of apical-basal polarity in alpha and beta cell fates *in vivo* (mice), we have yet to fully validate *in vivo* that this observation is mediated by the cAMP/PKA-CREB-EGR1-ARX signaling pathway.

### RESOURCE AVAILABILITY

#### Lead contact

Further information and requests for resources and reagents should be directed to and will be fulfilled by the lead contact, Henrik Semb ([henrik.semb@helmholtz-munich.de](mailto:henrik.semb@helmholtz-munich.de)).

#### Materials availability

All unique/stable reagents and the human ESC lines generated in this study are available from the [lead contact](#) with a completed materials transfer agreement.

#### Data and code availability

The scRNA-seq datasets (raw files and processed count matrices) have been deposited at GEO (Database: GSE224286). All codes used for analyzing scRNA-seq data are available on GitHub (<https://github.com/ITS-HMGU/Ulf-s-Project>; <https://doi.org/10.5281/zenodo.14628205>).

Any additional information required to reanalyze the data reported in this work paper is available from the [lead contact](#) upon request.

### ACKNOWLEDGMENTS

We are thankful to Julie Lee for performing CITE-seq library building and sequencing; to Jette Larsen, Diana Klüver, and Benoite Champon for their excellent technical support; to Anna Månsson and Paul Riccio for helping

with animal experiments; and to Gelo dela Cruz and Paul van Dieken for assistance with flow cytometry. Human fetal pancreas samples were kindly provided by Raphael Scharfmann. The NEUROG3-TagRFP reporter was a kind gift from Selcen Beydag-Tasöz from the University of Copenhagen. All the work is supported by the European Union's Horizon 2020 research and innovation program (ISLET, no. 874839), the Novo Nordisk Foundation Center for Stem Cell Biology (DanStem) at the University of Copenhagen (NNF grant, NNF17CC0027852) and the Helmholtz Zentrum München. U.T. received a research fellowship from the Deutsche Forschungsgemeinschaft (DFG project number 382408533). M.P. and J.S. are currently supported by the Novo Nordisk Foundation Center for Stem Cell Medicine (reNEW) at the University of Copenhagen (NNF grant, NNF21CC0073729).

### AUTHOR CONTRIBUTIONS

U.T., C.T., and H.S. conceived the project. U.T., C.T., F.H., and H.S. designed the experiments and interpreted the data. U.T., C.T., and F.H. performed most of the experiments and analyses. Individual contributions were as follows: M.P. analyzed CITE-seq data. E.S. generated CDH1 mutant cell lines and performed related experiments. I.K. contributed to cell line generation by piggy-Bac. Y.D. performed NEUROG3<sup>+</sup> sorting. J.S. supervised the CITE-seq experiments. U.T., C.T., and H.S. wrote the manuscript.

### DECLARATION OF INTERESTS

U.T., C.T., and H.S. are named as inventors in an international patent application, which is based on this work.

### STAR★METHODS

Detailed methods are provided in the online version of this paper and include the following:

- **KEY RESOURCES TABLE**
- **EXPERIMENTAL MODEL AND STUDY PARTICIPANT DETAILS**
  - Generation of transgenic Human embryonic stem cell (hESC) lines
  - Human fetal pancreas
  - The use of animals
- **METHOD DETAILS**
  - hESC culture and differentiation
  - Flow cytometry analysis and sorting
  - Immunofluorescence staining
  - Quantitative real-time PCR
  - Western blot
  - scRNA-seq sample preparation, library building, and analyses
  - *In Silico* transcription factor binding analysis
  - siRNA knockdown of *EGR1* and *DLK1*
  - cAMP ELISA
- **QUANTIFICATION AND STATISTICAL ANALYSIS**

### SUPPLEMENTAL INFORMATION

Supplemental information can be found online at <https://doi.org/10.1016/j.devcel.2025.02.008>.

Received: June 15, 2024

Revised: November 11, 2024

Accepted: February 14, 2025

Published: March 7, 2025

### REFERENCES

1. Russell, R., Carnese, P.P., Hennings, T.G., Walker, E.M., Russ, H.A., Liu, J.S., Giacometti, S., Stein, R., and Hebrok, M. (2020). Loss of the transcription factor MAFB limits beta-cell derivation from human PSCs. *Nat. Commun.* *11*, 2742. <https://doi.org/10.1038/s41467-020-16550-9>.
2. Lorberbaum, D.S., Kishore, S., Rosselot, C., Sarbaugh, D., Brooks, E.P., Aragon, E., Xuan, S., Simon, O., Ghosh, D., Mendelsohn, C., et al.

- (2020). Retinoic acid signaling within pancreatic endocrine progenitors regulates mouse and human beta cell specification. *Development* 147, dev189977. <https://doi.org/10.1242/dev.189977>.
3. Mastracci, T.L., Anderson, K.R., Papizan, J.B., and Sussel, L. (2013). Regulation of Neurod1 contributes to the lineage potential of Neurogenin3+ endocrine precursor cells in the pancreas. *PLoS Genet.* 9, e1003278. <https://doi.org/10.1371/journal.pgen.1003278>.
  4. Siehler, J., Blöchliger, A.K., Meier, M., and Lickert, H. (2021). Engineering islets from stem cells for advanced therapies of diabetes. *Nat. Rev. Drug Discov.* 20, 920–940. <https://doi.org/10.1038/s41573-021-00262-w>.
  5. Hoffman, B.D., Grashoff, C., and Schwartz, M.A. (2011). Dynamic molecular processes mediate cellular mechanotransduction. *Nature* 475, 316–323. <https://doi.org/10.1038/nature10316>.
  6. Panciera, T., Azzolin, L., Cordenonsi, M., and Piccolo, S. (2017). Mechanobiology of YAP and TAZ in physiology and disease. *Nat. Rev. Mol. Cell Biol.* 18, 758–770. <https://doi.org/10.1038/nrm.2017.87>.
  7. Vining, K.H., and Mooney, D.J. (2017). Mechanical forces direct stem cell behaviour in development and regeneration. *Nat. Rev. Mol. Cell Biol.* 18, 728–742. <https://doi.org/10.1038/nrm.2017.108>.
  8. Totaro, A., Panciera, T., and Piccolo, S. (2018). YAP/TAZ upstream signals and downstream responses. *Nat. Cell Biol.* 20, 888–899. <https://doi.org/10.1038/s41556-018-0142-z>.
  9. Larsen, H.L., and Grapin-Botton, A. (2017). The molecular and morphogenetic basis of pancreas organogenesis. *Semin. Cell Dev. Biol.* 66, 51–68. <https://doi.org/10.1016/j.semcdb.2017.01.005>.
  10. Kesavan, G., Sand, F.W., Greiner, T.U., Johansson, J.K., Kobberup, S., Wu, X., Brakebusch, C., and Semb, H. (2009). Cdc42-mediated tubulogenesis controls cell specification. *Cell* 139, 791–801. <https://doi.org/10.1016/j.cell.2009.08.049>.
  11. Villasenor, A., Chong, D.C., Henkemeyer, M., and Cleaver, O. (2010). Epithelial dynamics of pancreatic branching morphogenesis. *Development* 137, 4295–4305. <https://doi.org/10.1242/dev.052993>.
  12. Zhou, Q., Law, A.C., Rajagopal, J., Anderson, W.J., Gray, P.A., and Melton, D.A. (2007). A multipotent progenitor domain guides pancreatic organogenesis. *Dev. Cell* 13, 103–114. <https://doi.org/10.1016/j.devcel.2007.06.001>.
  13. Nyeng, P., Heilmann, S., Löf-Öhlin, Z.M., Pettersson, N.F., Hermann, F.M., Reynolds, A.B., and Semb, H. (2019). p120ctn-Mediated Organ Patterning Precedes and Determines Pancreatic Progenitor Fate. *Dev. Cell* 49, 31–47.e9. <https://doi.org/10.1016/j.devcel.2019.02.005>.
  14. Mamidi, A., Prawiro, C., Seymour, P.A., de Lichtenberg, K.H., Jackson, A., Serup, P., and Semb, H. (2018). Mechanosignalling via integrins directs fate decisions of pancreatic progenitors. *Nature* 564, 114–118. <https://doi.org/10.1038/s41586-018-0762-2>.
  15. Gradwohl, G., Dierich, A., LeMour, M., and Guillemot, F. (2000). neurogenin3 is required for the development of the four endocrine cell lineages of the pancreas. *Proc. Natl. Acad. Sci. USA* 97, 1607–1611. <https://doi.org/10.1073/pnas.97.4.1607>.
  16. Gu, G., Dubauskaite, J., and Melton, D.A. (2002). Direct evidence for the pancreatic lineage: NGN3+ cells are islet progenitors and are distinct from duct progenitors. *Development* 129, 2447–2457. <https://doi.org/10.1242/dev.129.10.2447>.
  17. Jennings, R.E., Berry, A.A., Strutt, J.P., Gerrard, D.T., and Hanley, N.A. (2015). Human pancreas development. *Development* 142, 3126–3137. <https://doi.org/10.1242/dev.120063>.
  18. McGrath, P.S., Watson, C.L., Ingram, C., Helmuth, M.A., and Wells, J.M. (2015). The Basic Helix-Loop-Helix Transcription Factor NEUROG3 Is Required for Development of the Human Endocrine Pancreas. *Diabetes* 64, 2497–2505. <https://doi.org/10.2337/db14-1412>.
  19. Löf-Öhlin, Z.M., Nyeng, P., Bechard, M.E., Hess, K., Bankaitis, E., Greiner, T.U., Ameri, J., Wright, C.V., and Semb, H. (2017). EGFR signalling controls cellular fate and pancreatic organogenesis by regulating apicalbasal polarity. *Nat. Cell Biol.* 19, 1313–1325. <https://doi.org/10.1038/ncb3628>.
  20. Johansson, K.A., Dursun, U., Jordan, N., Gu, G., Beermann, F., Gradwohl, G., and Grapin-Botton, A. (2007). Temporal control of neurogenin3 activity in pancreas progenitors reveals competence windows for the generation of different endocrine cell types. *Dev. Cell* 12, 457–465. <https://doi.org/10.1016/j.devcel.2007.02.010>.
  21. Bankaitis, E.D., Bechard, M.E., and Wright, C.V.E. (2015). Feedback control of growth, differentiation, and morphogenesis of pancreatic endocrine progenitors in an epithelial plexus niche. *Genes Dev.* 29, 2203–2216. <https://doi.org/10.1101/gad.267914.115>.
  22. Capaldo, C.T., and Macara, I.G. (2007). Depletion of E-cadherin disrupts establishment but not maintenance of cell junctions in Madin-Darby canine kidney epithelial cells. *Mol. Biol. Cell* 18, 189–200. <https://doi.org/10.1091/mbc.e06-05-0471>.
  23. Larue, L., Ohsugi, M., Hirchenhain, J., and Kemler, R. (1994). E-cadherin null mutant embryos fail to form a trophectoderm epithelium. *Proc. Natl. Acad. Sci. USA* 91, 8263–8267. <https://doi.org/10.1073/pnas.91.17.8263>.
  24. Wang, F., Dumstrei, K., Haag, T., and Hartenstein, V. (2004). The role of DE-cadherin during cellularization, germ layer formation and early neurogenesis in the Drosophila embryo. *Dev. Biol.* 270, 350–363. <https://doi.org/10.1016/j.ydbio.2004.03.002>.
  25. Gumbiner, B., Stevenson, B., and Grimaldi, A. (1988). The role of the cell adhesion molecule uvomorulin in the formation and maintenance of the epithelial junctional complex. *J. Cell Biol.* 107, 1575–1587. <https://doi.org/10.1083/jcb.107.4.1575>.
  26. Davis, M.A., Ireton, R.C., and Reynolds, A.B. (2003). A core function for p120-catenin in cadherin turnover. *J. Cell Biol.* 163, 525–534. <https://doi.org/10.1083/jcb.200307111>.
  27. Gottardi, C.J., Wong, E., and Gumbiner, B.M. (2001). E-cadherin suppresses cellular transformation by inhibiting beta-catenin signaling in an adhesion-independent manner. *J. Cell Biol.* 153, 1049–1060. <https://doi.org/10.1083/jcb.153.5.1049>.
  28. Rezaia, A., Bruin, J.E., Arora, P., Rubin, A., Batushansky, I., Asadi, A., O'Dwyer, S., Quiskamp, N., Mojibian, M., Albrecht, T., et al. (2014). Reversal of diabetes with insulin-producing cells derived in vitro from human pluripotent stem cells. *Nat. Biotechnol.* 32, 1121–1133. <https://doi.org/10.1038/nbt.3033>.
  29. Russ, H.A., Parent, A.V., Ringler, J.J., Hennings, T.G., Nair, G.G., Shveygert, M., Guo, T., Puri, S., Haataja, L., Cirulli, V., et al. (2015). Controlled induction of human pancreatic progenitors produces functional beta-like cells in vitro. *EMBO J.* 34, 1759–1772. <https://doi.org/10.15252/emboj.201591058>.
  30. Veres, A., Faust, A.L., Bushnell, H.L., Engquist, E.N., Kenty, J.H.R., Harb, G., Poh, Y.C., Sintov, E., Gürtler, M., Pagliuca, F.W., et al. (2019). Charting cellular identity during human in vitro beta-cell differentiation. *Nature* 569, 368–373. <https://doi.org/10.1038/s41586-019-1168-5>.
  31. Petersen, M.B.K., Azad, A., Ingvorsen, C., Hess, K., Hansson, M., Grapin-Botton, A., and Honoré, C. (2017). Single-Cell Gene Expression Analysis of a Human ESC Model of Pancreatic Endocrine Development Reveals Different Paths to beta-Cell Differentiation. *Stem Cell Rep.* 9, 1246–1261. <https://doi.org/10.1016/j.stemcr.2017.08.009>.
  32. Corbeil, D., Marzesco, A.M., Fargeas, C.A., and Huttner, W.B. (2010). Prominin-1: a distinct cholesterol-binding membrane protein and the organisation of the apical plasma membrane of epithelial cells. *Subcell. Biochem.* 51, 399–423. [https://doi.org/10.1007/978-90-481-8622-8\\_14](https://doi.org/10.1007/978-90-481-8622-8_14).
  33. Lorentzen, A., Becker, P.F., Kosla, J., Saini, M., Weidele, K., Ronchi, P., Klein, C., Wolf, M.J., Geist, F., Seubert, B., et al. (2018). Single cell polarity in liquid phase facilitates tumour metastasis. *Nat. Commun.* 9, 887. <https://doi.org/10.1038/s41467-018-03139-6>.
  34. Beydag-Tasöz, B.S., D'Costa, J.V., Hersemann, L., Lee, B.H., Luppino, F., Kim, Y.H., Zechner, C., and Grapin-Botton, A. (2023). Integrating single-cell imaging and RNA sequencing datasets links differentiation and morphogenetic dynamics of human pancreatic endocrine progenitors. *Dev. Cell* 58, 2292–2308.e6. <https://doi.org/10.1016/j.devcel.2023.07.019>.

35. Stoeckius, M., Hafemeister, C., Stephenson, W., Houck-Loomis, B., Chattopadhyay, P.K., Swerdlow, H., Satija, R., and Smibert, P. (2017). Simultaneous epitope and transcriptome measurement in single cells. *Nat. Methods* *14*, 865–868. <https://doi.org/10.1038/nmeth.4380>.
36. van Gurp, L., Fodoulian, L., Oropeza, D., Furuyama, K., Bru-Tari, E., Vu, A.N., Kaddis, J.S., Rodríguez, I., Thorel, F., and Herrera, P.L. (2022). Generation of human islet cell type-specific identity genesets. *Nat. Commun.* *13*, 2020. <https://doi.org/10.1038/s41467-022-29588-8>.
37. Xu, E.E., Krentz, N.A.J., Tan, S., Chow, S.Z., Tang, M., Nian, C., and Lynn, F.C. (2015). SOX4 cooperates with neurogenin 3 to regulate endocrine pancreas formation in mouse models. *Diabetologia* *58*, 1013–1023. <https://doi.org/10.1007/s00125-015-3507-x>.
38. Wilson, M.E., Yang, K.Y., Kalousova, A., Lau, J., Kosaka, Y., Lynn, F.C., Wang, J., Mrejen, C., Episkopou, V., Clevers, H.C., et al. (2005). The HMG box transcription factor Sox4 contributes to the development of the endocrine pancreas. *Diabetes* *54*, 3402–3409. <https://doi.org/10.2337/diabetes.54.12.3402>.
39. Ma, Z., Zhang, X., Zhong, W., Yi, H., Chen, X., Zhao, Y., Ma, Y., Song, E., and Xu, T. (2023). Deciphering early human pancreas development at the single-cell level. *Nat. Commun.* *14*, 5354. <https://doi.org/10.1038/s41467-023-40893-8>.
40. Collombat, P., Mansouri, A., Hecksher-Sorensen, J., Serup, P., Krull, J., Gradwohl, G., and Gruss, P. (2003). Opposing actions of Arx and Pax4 in endocrine pancreas development. *Genes Dev.* *17*, 2591–2603. <https://doi.org/10.1101/gad.269003>.
41. Daily, K., Patel, V.R., Rigor, P., Xie, X., and Baldi, P. (2011). MotifMap: integrative genome-wide maps of regulatory motif sites for model species. *BMC Bioinformatics* *12*, 495. <https://doi.org/10.1186/1471-2105-12-495>.
42. Xie, X., Rigor, P., and Baldi, P. (2009). MotifMap: a human genome-wide map of candidate regulatory motif sites. *Bioinformatics* *25*, 167–174. <https://doi.org/10.1093/bioinformatics/btn605>.
43. Leu, S.Y., Kuo, L.H., Weng, W.T., Lien, I.C., Yang, C.C., Hsieh, T.T., Cheng, Y.N., Chien, P.H., Ho, L.C., Chen, S.H., et al. (2020). Loss of EGR-1 uncouples compensatory responses of pancreatic beta cells. *Theranostics* *10*, 4233–4249. <https://doi.org/10.7150/thno.40664>.
44. Thiel, G., Müller, I., and Rössler, O.G. (2014). Expression, signaling and function of Egr transcription factors in pancreatic beta-cells and insulin-responsive tissues. *Mol. Cell. Endocrinol.* *388*, 10–19. <https://doi.org/10.1016/j.mce.2014.03.001>.
45. Ameri, J., Borup, R., Prawiro, C., Ramond, C., Schachter, K.A., Scharfmann, R., and Semb, H. (2017). Efficient Generation of Glucose-Responsive Beta Cells from Isolated GP2<sup>+</sup> Human Pancreatic Progenitors. *Cell Rep.* *19*, 36–49. <https://doi.org/10.1016/j.celrep.2017.03.032>.
46. Du, Y., Liang, Z., Wang, S., Sun, D., Wang, X., Liew, S.Y., Lu, S., Wu, S., Jiang, Y., Wang, Y., et al. (2022). Human pluripotent stem-cell-derived islets ameliorate diabetes in non-human primates. *Nat. Med.* *28*, 272–282. <https://doi.org/10.1038/s41591-021-01645-7>.
47. Liu, H., Li, R., Liao, H.K., Min, Z., Wang, C., Yu, Y., Shi, L., Dan, J., Hayek, A., Martinez Martinez, L., et al. (2021). Chemical combinations potentiate human pluripotent stem cell-derived 3D pancreatic progenitor clusters toward functional beta cells. *Nat. Commun.* *12*, 3330. <https://doi.org/10.1038/s41467-021-23525-x>.
48. Lamba, A., and Zernicka-Goetz, M. (2023). The role of polarization and early heterogeneities in the mammalian first cell fate decision. *Curr. Top. Dev. Biol.* *154*, 169–196. <https://doi.org/10.1016/bs.ctdb.2023.02.006>.
49. Hirate, Y., Hirahara, S., Inoue, K.I., Suzuki, A., Alarcon, V.B., Akimoto, K., Hirai, T., Hara, T., Adachi, M., Chida, K., et al. (2013). Polarity-dependent distribution of angiominin localizes Hippo signaling in preimplantation embryos. *Curr. Biol.* *23*, 1181–1194. <https://doi.org/10.1016/j.cub.2013.05.014>.
50. Nishioka, N., Inoue, K., Adachi, K., Kiyonari, H., Ota, M., Ralston, A., Yabuta, N., Hirahara, S., Stephenson, R.O., Ogonuki, N., et al. (2009). The Hippo signaling pathway components Lats and Yap pattern Tead4 activity to distinguish mouse trophectoderm from inner cell mass. *Dev. Cell* *16*, 398–410. <https://doi.org/10.1016/j.devcel.2009.02.003>.
51. Chartier, F.J.M., Hardy, É.J.L., and Laprise, P. (2011). Crumbs controls epithelial integrity by inhibiting Rac1 and PI3K. *J. Cell Sci.* *124*, 3393–3398. <https://doi.org/10.1242/jcs.092601>.
52. Clark, B.S., Cui, S., Miesfeld, J.B., Klezovitch, O., Vasioukhin, V., and Link, B.A. (2012). Loss of Lgl1 in retinal neuroepithelia reveals links between apical domain size, Notch activity and neurogenesis. *Development* *139*, 1599–1610. <https://doi.org/10.1242/dev.078097>.
53. Ossipova, O., Ezan, J., and Sokol, S.Y. (2009). PAR-1 phosphorylates Mind bomb to promote vertebrate neurogenesis. *Dev. Cell* *17*, 222–233. <https://doi.org/10.1016/j.devcel.2009.06.010>.
54. Ohata, S., Aoki, R., Kinoshita, S., Yamaguchi, M., Tsuruoka-Kinoshita, S., Tanaka, H., Wada, H., Watabe, S., Tsuboi, T., Masai, I., et al. (2011). Dual roles of Notch in regulation of apically restricted mitosis and apicobasal polarity of neuroepithelial cells. *Neuron* *69*, 215–230. <https://doi.org/10.1016/j.neuron.2010.12.026>.
55. Lau, H.H., Krentz, N.A.J., Abaitua, F., Perez-Alcantara, M., Chan, J.W., Ajeian, J., Ghosh, S., Lee, Y., Yang, J., Thaman, S., et al. (2023). PAX4 loss of function increases diabetes risk by altering human pancreatic endocrine cell development. *Nat. Commun.* *14*, 6119. <https://doi.org/10.1038/s41467-023-41860-z>.
56. Gage, B.K., Asadi, A., Baker, R.K., Webber, T.D., Wang, R., Itoh, M., Hayashi, M., Miyata, R., Akashi, T., and Kieffer, T.J. (2015). The role of ARX in Human Pancreatic Endocrine Specification. *PLoS One* *10*, e0144100. <https://doi.org/10.1371/journal.pone.0144100>.
57. Zhu, Z., Li, Q.V., Lee, K., Rosen, B.P., González, F., Soh, C.L., and Huangfu, D. (2016). Genome Editing of Lineage Determinants in Human Pluripotent Stem Cells Reveals Mechanisms of Pancreatic Development and Diabetes. *Cell Stem Cell* *18*, 755–768. <https://doi.org/10.1016/j.stem.2016.03.015>.
58. Lee, H., Yu, D.M., Park, J.S., Lee, H., Kim, J.S., Kim, H.L., Koo, S.H., Lee, J.S., Lee, S., and Ko, Y.G. (2020). Prominin-1-Radixin axis controls hepatic gluconeogenesis by regulating PKA activity. *EMBO Rep.* *21*, e49416. <https://doi.org/10.15252/embr.201949416>.
59. Kim, J.S., Han, H.S., Seong, J.K., Ko, Y.G., and Koo, S.H. (2023). Involvement of a novel cAMP signaling mediator for beige adipogenesis. *Metabolism* *143*, 155536. <https://doi.org/10.1016/j.metabol.2023.155536>.

## STAR★METHODS

### KEY RESOURCES TABLE

REAGENT or RESOURCE	SOURCE	IDENTIFIER
<b>Antibodies</b>		
INSULIN	Dako/Agilent	#A0564; RRID: AB_10013624
GLUCAGON	Cell Signaling	#8233; RRID: AB_10859908
EZRIN	Abcam	#ab4069; RRID: AB_304261
Beta-catenin	Santa Cruz	#sc-7199; RRID: AB_634603
ZO-1	Thermo Fisher	#40-2200; RRID: AB_2533456
CDH1 (E-cadherin)	Takara Bio	#M108; RRID: AB_2895157
NEUROG3	R&D Systems	#AF3444; RRID: AB_2149527
PROM1 (CD133)	Miltenyi	#130-090-422; RRID: AB_244339
PDX1	R&D Systems	#AF2419; RRID: AB_355257
LAM	Sigma-Aldrich	#L9393; RRID: AB_477163
aPKC	Santa Cruz	#sc-216; RRID: AB_2300359
MUC1	Thermo Fisher	#MA5-11202; RRID: AB_11000874
mCherry	Novus	#NBP1-96752; RRID: AB_11034849
EGFP/YFP	Abcam	#ab5450; RRID: AB_304897
tRFP/mKATE2	Evrogen	#ab233; RRID: AB_2571743
ARX	R&D System	#AF7068; RRID: AB_10973178
CREB	Cell Signaling	#4820; RRID: AB_1903940
Phospho-CREB (Ser133)	Cell Signaling	#9198; RRID: AB_2561044
EGR1	Proteintech	#22008-1-AP; RRID: AB_11182923
GAPDH	R&D Systems	#AF5718; RRID: AB_2278695
Alexa fluor 647 anti-INSULIN	BD Pharmingen	#565689; RRID: AB_2739331
PE anti-GLUCAGON	BD Pharmingen	#565860; RRID: AB_2739382
BV421 anti-GLUCAGON	BD Pharmingen	#565891; RRID: AB_2739385
APC anti-PROM1 (CD133)	Miltenyi	#130-098-898; RRID: AB_2725935
<b>Bacterial strains</b>		
MAX Efficiency DH5a T1 Phage Resistant Competent Cells	Thermo Fisher	#12034013
One Shot™ OmniMAX™ 2 T1R Chemically Competent E. coli	Thermo Fisher	# C854003
<b>Biological samples</b>		
Human fetal pancreatic tissue	French Institute of Health and Medical Research, Paris, France	N/A
<b>Chemicals, peptides, and recombinant proteins</b>		
CHIR99021	Axon Medchem	#1386
Activin A	PeproTech	#120-14
KGF	PeproTech	#100-19
Vitamin C	Sigma Aldrich	#A4403
LDN193189	Tebu Tech	#04-0074-10
SANT1	Sigma Aldrich	#S4572
Retinoic acid	Sigma Aldrich	#R2625
TBP	Calbiochem	#565740
ALK5iil	Santa Cruz	#sc-221234A
γSec-iXX	Merck Millipore	#565789

(Continued on next page)

**Continued**

REAGENT or RESOURCE	SOURCE	IDENTIFIER
Latrunculin B	Sigma Aldrich	#L5288
Heparin	Sigma Aldrich	#H3149-100KU
Bovine serum albumin (BSA)	Proliant	#7500804
Bovine serum albumin (BSA)	Roche	#10775835001
Bovine serum albumin (BSA)	Sigma Aldrich	#B4287
Y-27632	Merck Millipore	#688000
45 % glucose solution in water	Sigma Aldrich	#G8769
7.5% sodium bicarbonate solution	Thermo Fisher	#25080094
Forskolin	Sigma Aldrich	#F6886
3-Isobutyl-1-methylxanthin	Thermo Fisher	#J64598.MC
G418	Thermo Fisher	#10131027
Hygromycin	Thermo Fisher	#10687010
Doxycycline	Sigma-Aldrich	#D3447
<b>Critical commercial assays</b>		
RNeasy Mini Kit	Qiagen	#74106
RNeasy Micro Kit	Qiagen	#74004
iScript cDNA Synthesis Kit	BIO-RAD	#1708891
KAPA HiFi HotStart Library Amplification Kit	Roche	#07958951001
cAMP XP <sup>®</sup> Assay Kit	Cell Signaling	#4339
P3 Primary Cell Kit	Lonza	#V4XP-3024
LIVE/DEAD <sup>™</sup> Fixable Violet Dead Cell Stain Kit	Thermo Fisher	#L34964
<b>Deposited data</b>		
scRNA-seq datasets	This paper	GSE224286
<b>Experimental models: Cell lines</b>		
SA121	Takara bio	N/A
H1	Beydag-Tasöz et al. <sup>34</sup> (University of Copenhagen)	N/A
<b>Experimental models: Organisms/strains</b>		
<i>Cdc42<sup>fl/fl</sup></i> R26-YFP <sup>+/+</sup> mice	In house	N/A
<i>Pdx1-Cre<sup>+/-</sup></i> <i>Cdc42<sup>fl/wt</sup></i> mice	In house	N/A
<b>Oligonucleotides</b>		
siRNA against EGR1	Thermo Fisher	#S4537; #S4538
Negative control siRNA	Thermo Fisher	#4390843
<b>Recombinant DNA</b>		
Mutant CDH1 sequences	Addgene	#45770; #45773
PiggyBac destination vector PB-TAC-ERN	Addgene	#80475
Cas9 expression vector (pX458-HF1)	Addgene	#48138
<b>Software and algorithms</b>		
Adobe Photoshop 2022	Adobe	<a href="https://www.adobe.com">https://www.adobe.com</a>
Adobe Illustrator 2023	Adobe	<a href="https://www.adobe.com">https://www.adobe.com</a>
Imaris 8.4, 9.0	Oxford Instruments	<a href="https://imaris.oxinst.com/">https://imaris.oxinst.com/</a>
Fiji 2.0/ImageJ	NIH Image	<a href="http://imagej.nih.gov/ij">http://imagej.nih.gov/ij</a>
GraphPad Prism 10	GraphPad	<a href="https://www.graphpad.com">https://www.graphpad.com</a>
FlowJo 10	BD	<a href="https://www.flowjo.com">https://www.flowjo.com</a>
FCS Express <sup>™</sup> 7	De Novo Software	<a href="https://denovosoftware.com">https://denovosoftware.com</a>
ZEN (blue edition)	ZEISS	<a href="https://www.micro-shop.zeiss.com">https://www.micro-shop.zeiss.com</a>

## EXPERIMENTAL MODEL AND STUDY PARTICIPANT DETAILS

### Generation of transgenic Human embryonic stem cell (hESC) lines

CDH1 mutant cell lines: The mutant CDH1 sequences<sup>27</sup> (Addgene #45770 and #45773) were cloned into the piggyBac destination vector PB-TAC-ERN (Addgene #80475) for doxycycline induction and mCherry co-expression using Gateway technology (Thermo Fisher). A piggyBac transposase vector (System Biosciences) was co-transfected for the generation of CDH1ΔE and CDH1ΔP.

EZR-mKATE2/NEUROG3-EGFP double reporter cell line: The EZR sequence, including 1,000 bp homology arms, was amplified from human genomic DNA and cloned into a pBluescriptSK vector backbone using Seamless cloning (Thermo Fisher) to generate the EZR-mKATE2 fusion cassette. Two guide-RNA sequences targeting the EZR locus were cloned into a Cas9 expression vector (pX458-HF1, Addgene #48138) and co-transfected.

Plasmids (1–5 μg/10<sup>6</sup> cells) were transfected into hESCs by the P3 Primary Cell Kit (Lonza) using the CA137 program on the Lonza 4D-Nucleofector. Transfected cells were selected by 100 μg/ml G418 (Thermo Fisher) or 50 μg/ml hygromycin (Thermo Fisher) for 1–3 days, and single colonies were manually picked to generate clonal cell lines. Inducible cell lines were treated with 2 μg/ml doxycycline (Sigma-Aldrich).

### Human fetal pancreas

Fixed human fetal pancreatic tissue (sex unknown) was supplied by Raphael Scharfmann, French Institute of Health and Medical Research, Paris, France. The use of human tissue was approved by “French Agence de Biomedecine” (accreditation # PFS08-011) and informed consent was obtained from all donors for the use of these human tissues in research.

### The use of animals

Mouse pancreatic dissection, fixation, sectioning, and embedding were performed as previously described.<sup>10</sup>

Mice were housed at the University of Copenhagen under controlled conditions in specific-pathogen-free (SPF) facilities. These mice were housed at 2h light/dark cycles at a room temperature of 22°C (± 2°C) and a humidity of 55% (±10%), with the air in the room changed 8–10 times per hour. Food and water were provided ad libitum. Mice were healthy and routinely genotyped.

All experiments were performed according to guidelines and ethics approved by the Danish Animal Experiments Inspectorate (Dyreforsøgstilsynet). Data were collected from both male and female embryos.

## METHOD DETAILS

### hESC culture and differentiation

hESCs were cultivated on dishes coated with hESC-qualified Matrigel (Corning) in mTESR1 medium (Stemcell Technologies) at 37 °C and 5% CO<sub>2</sub> and passaged using TrypLE (Thermo Fisher) and 10 μM ROCK inhibitor Y-27632 (Merck Millipore).

Unless otherwise stated, all experiments were conducted with the wild-type hESC cell line SA121 (Takara Bio), which was also used to generate the inducible overexpression cell lines CDH1ΔE and CDH1ΔP. The NEUROG3-eGFP reporter<sup>19</sup> is likewise based on SA121 and was used to generate the EZR-mKATE2/NEUROG3-eGFP double reporter cell line. NEUROG3-tagRFPT/EGFP double reporter cell line generated based on wild-type hESC cell line H1.<sup>34</sup>

For Matrigel overlay differentiation, 130,000–150,000 cells/cm<sup>2</sup> were seeded in an ice-cold dilution of 33% (v/v) growth factor reduced Matrigel (Corning) in mTESR1 medium plus 10 μM ROCK inhibitor and placed at 4°C for 20–30 min to allow the cells to settle before matrix solidification was induced at 37°C. The next day, liquid mTESR1 medium was added. Daily media changes were performed manually with great caution to avoid disturbing the delicate matrix, and a washing step with PBS (Thermo Fisher) was included.

The directed differentiation toward pancreatic endocrine cells can be divided into six stages (S1–S6) with distinct media based on a previous study<sup>28</sup> with modifications as indicated. Two days after cell seeding, the medium was shifted to S1 differentiation medium for 3 days, containing 100 ng/ml Activin A (PeproTech; replacing GDF8) and CHIR-99021 (AxonMedChem; 3 μM on day 1, 0.3 μM on day 2, withdrawal on day 3). Unless otherwise stated, the remaining stages followed the standard durations and media compositions<sup>28</sup>: S2 (2 days), S3 (2 days), S4 (3 days), S5 (3 days), S6 (4–7 days). For synchronized endocrinogenesis, S4 medium was supplemented for 2 days with 0.1 μM γSec-iXX (Merck Millipore), 1 μM Latrunculin B (Sigma-Aldrich), and 10 μM ALK5iil (Santa Cruz) after either one day (early induction) or four days (late induction) in standard S4 medium, followed by 7 days of basal S4 medium without cytokines.<sup>28</sup>

### Flow cytometry analysis and sorting

Cells were retrieved from Matrigel overlay cultures using Cell Recovery Solution (Corning) and dissociated by TrypLE treatment and straining (50 μM). Sorting of living cells was performed on a BD FACS Aria III sorter after staining with an APC-conjugated PROM1-antibody (1:10) with gating for single (scatter characteristics), living (DAPI<sup>+</sup>) cells based on single-color isotype and unstained controls in 0.5% fatty acid-free BSA/PBS.

Flow cytometry quantification of fixed, stained cells was performed as previously described<sup>19</sup> on a BD LSR Fortessa analyzer or Miltenyi MACSQuant analyzer. Antibodies are listed in the [key resources table](#).

### Immunofluorescence staining

Fixation and immunological staining of hESC and mouse material were performed as previously described.<sup>14,19</sup> Human fetuses (9–12.5 weeks post conception) were staged by foot length. The pancreas was dissected from the gut and stomach, fixed in 3.7% formalin for 72h, and embedded in paraffin. Longitudinal sections (4–8  $\mu$ m) were cut on a microtome. For immunological staining, sections were cleared of paraffin by sequential washing in xylene, ethanol, and water. Antigen retrieval was performed in TE buffer (10 mM Tris, 1 mM EDTA, 0.05% Tween20, pH 9.0) at 95 °C for 20 min, followed by quenching with 3% hydrogen peroxidase for 7 min, permeabilization by 0.3% Triton X-100 and blocking for 1 h in a TSA amplification buffer (Perkin Elmer). Primary antibodies are listed in the [key resources table](#). All Alexa Fluor-conjugated secondary antibodies (Thermo Fisher) were used as 1: 500 dilutions.

Samples were imaged with Zeiss LSM780, Zeiss LSM880, CellDiscoverer 7, or Leica SP8 confocal microscopes. Image analysis, segmentation, and quantification were performed with Fiji (ImageJ) and Imaris (Oxford Instruments).

### Quantitative real-time PCR

Total RNA was extracted using the RNeasy Mini Kit (Qiagen, Cat#74106) or RNeasy Micro Kit (Qiagen, Cat#74004). According to the manufacturer's instructions, reverse transcription was performed with iScript cDNA Synthesis Kit (BIO-RAD, Cat#1708891). Real-time PCR measurements were performed in technical duplicates using the QuantStudio 7 Flex Real-Time-PCR-System (Thermo Fisher) with TaqMan FAM probes (Thermo Fisher) with TaqMan Master Mix (Thermo Fisher, Cat#4364103) or primers (Integrated DNA Technologies) with SYBR Green PCR Master Mix (Thermo Fisher, Cat#4309155). Relative gene expression was determined using the housekeeping genes *GAPDH*. TaqMan probes and primers are listed in [Table S1](#).

### Western blot

Cells were washed twice in PBS, collected, and lysed in RIPA buffer (Thermo Fisher, Cat#8990) on ice for 30 min and then sonicated for 1 min at 5 s intervals. After centrifugation at 10,000 *g* at 4 °C for 10 min, the supernatant was transferred into new tubes. The concentration of the cell protein sample was measured by bicinchoninic acid, and protein samples were boiled in an SDS sample buffer at 95 °C for 5 min. The cell extract sample was resolved by 10% Acr-Bis SDS-PAGE and transferred to polyvinylidene difluoride membranes (PVDF, Merck Millipore). Nonspecific binding was blocked by incubation in 3% non-fat milk in TBS at room temperature for 1 h. Blots were then probed with primary antibodies overnight by incubation at 4 °C with anti-ARX, anti-EGR1, anti-CREB or anti-pCREB. GAPDH served as a loading control. Immunoreactivity bands were then probed for 1 h at room temperature with horseradish peroxidase (HRP)-conjugated secondary antibodies. Protein bands were detected by Chemiluminescent HRP substrate (Thermo Fisher, Cat#34579) or 1-step ultra TMB blotting solution (Thermo Fisher, Cat#37574). Protein bands were quantified by densitometry using Fiji (ImageJ) software.

### scRNA-seq sample preparation, library building, and analyses

The sample preparation was performed as previously described.<sup>35</sup> Briefly, non-polarized (PROM1<sup>-</sup>) and polarized (PROM1<sup>+</sup>) cells from three independent late-induced differentiation cultures were purified by flow cytometry for PROM1. Early-induced and late-induced cells, as well as purified non-polarized late and polarized cells, were then barcoded with unique Oligonucleotide Hash Tags (early, CAG TAG TCA CGG TCA; late, ATT GAC CCG CGT TAG; polarized, TAA CGA CCA GCC ATA; non-polarized, AAA TCT CTC AGG CTC). After Hash- and CITE-tagged cells were counted and checked for viability using a hemacytometer, 25,000 cells were loaded into a Chromium Controller (10X Genomics). The library was prepared using the Chromium Single Cell 3' v2 protocol (10X Genomics). Indexed cDNAs were then pooled and amplified by PCR according to the Chromium Single Cell 3' v2 protocol (10X Genomics) and with specific primers amplifying the antibody-derived tags. The single cell 3' v2 protocol (10X Genomics) was used for the mRNA-derived cDNA library preparation, and the KAPA HiFi HotStart Library Amplification Kit (Roche) was used for the antibody-derived tagged library. Following the final bead purification, all the libraries were pooled together and sequenced using Illumina NextSeq 500.

For analysis, raw reads were pre-processed using the 10X genomics Cell Ranger pipeline. The reads were aligned to the GRCh38 2020-A genome. cDNA reads were used to construct a count matrix, while HTO reads were used to count HTO tags using the CITE-seq-Count-1.4.3 tool. Further downstream analysis with integration was done using both Seurat and Scanpy.

In the analysis for [Figure 5A](#), a Venn diagram was used to identify overlapping differentially expressed genes between polarized EPs (versus non-polarized EPs) and early beta cells (versus early alpha cells), as well as between non-polarized EPs (versus polarized EPs) and early alpha cells (versus early beta cells). The list of differentially expressed genes is provided in [Table S3](#).

### In Silico transcription factor binding analysis

The Gene Search function of the online tool at <http://motifmap.ics.uci.edu><sup>41,42</sup> was employed to search for transcription factor binding sites 2,000 base pairs upstream and downstream of the transcriptional start site of *ARX*.

### siRNA knockdown of *EGR1* and *DLK1*

The end of S4 cells (at day 10) were dissociated to single cells as described above and reverse transfected with 50 nM of two siRNA against *EGR1* (Thermo Fisher, ID# S4537 and S4538) or 50 nM of three siRNA against *DLK1* (Thermo Fisher, ID# S16738, S16739 and S16740) or 100/150 nM negative control siRNA (Thermo Fisher, Cat# 4390843) using Lipofectamine RNAiMAX (Thermo Fisher, Cat# 13778030). In brief, in a 24-well format, 2  $\mu$ l RNAiMAX was premixed with siRNA(s) in 100  $\mu$ l OptiMEM medium (Thermo Fisher,

Cat# 31985070), and 20-30 minutes later, 500,000 cells per  $\text{cm}^2$  were added in 400  $\mu\text{l}$  S5 medium supplemented with 10  $\mu\text{M}$  ROCK inhibitor. 24-48 hrs after transfection, cells were harvested for transcriptional analyses. On Day 13, the S5 medium was switched to basal medium for 4 days for flow cytometry analyses.

#### **cAMP ELISA**

The sample preparation was performed according to the protocol instructions of the cAMP XP Assay Kit (Cell Signaling). Briefly, sorted cells were rinsed with 200  $\mu\text{l}$  ice-cold PBS and then 100  $\mu\text{l}$  1X lysis buffer was added. The samples were incubated on ice for 10 min for analysis.

#### **QUANTIFICATION AND STATISTICAL ANALYSIS**

Statistical analyses were performed with GraphPad Prism (version 10.0, GraphPad Software). Unless otherwise noted, a paired nonparametric test (Wilcoxon matched-pairs signed-rank test) was used to assess significance. Asterisks denote p-values as follows: \*  $p < 0.05$ ; \*\*  $p < 0.01$ ; \*\*\*  $p < 0.001$ . Each n represents a biological replicate (mice or independent experiments). Data figures illustrate the mean with standard deviation and the values of individual biological replicates.